A Rock and Paleomagnetic Characterization of the Duluth Complex Layered Series Intrusions Associated with the Nokomis Deposit in NE Minnesota.

A THESIS
SUBMITTED TO THE FACULTY OF THE GRADUATE SCHOOL
OF THE UNIVERSITY OF MINNESOTA
BY

Evan Michael Finnes

IN PARTIAL FULFILLMENT OF THE REQUIREMENTS
FOR THE DEGREE OF
MASTER OF SCIENCE

Joshua M. Feinberg

June 2012

Acknowledgements

It is almost impossible for me to put into words the level of gratitude that I have for everyone who assisted me throughout this project. First of all, thanks to my awesome advisor, Joshua Feinberg, whose invaluable guidance, and extensive knowledge has kept me on-track and was able to find amazing opportunities for me. Thanks to everyone at the Institute for Rock Magnetism. Specifically, Mike Jackson, Peter Solheid, and Julie Bowles for their assistance with both concept and equipment. Thanks to the University of Minnesota, and to the amazing staff at the Department of Earth Sciences. I would like to thank Paul Weiblen for the many conversations we had about the Duluth Complex. Thanks to Jim Miller and the Precambrian Research Center for financial support. Thanks to Maxwell Brown for assistance in the field, and advice on this project. I would also like to thank Calvin Alexander, Bruce Moskowitz, and Josh Feinberg for participating in my defense committee.

I would also like to thank the entire gang at Duluth Metals for both financial support, and for the opportunity to work on this project. Especially Dean Peterson whose enthusiasm for this project has been much appreciated.

I would like to thank my wife, Jinah, for her incredible patience and moral support. I would also like to thank my parents for their continual encouragement and to my children, Aidan and Anika for always keeping a smile on my face.

Dedication

I dedicate this thesis to my wonderful wife, Jinah Ellyn Finnes, who has been unbelievably patient with me over the last few years. Thank you.

Abstract

The Bald Eagle Intrusion (BEI), Nickel Lake Macrodike (NLMD), and the South Kawishiwi Intrusion (SKI) are mafic intrusions related to the Layered Series rocks of the Duluth Complex, which formed approximately 1.1 billion years ago as part of the Midcontinet Rift. These intrusions represent a complex plumbing system and the economically important minerals within them are collectively referred to as the Nokomis Deposit. The model proposed by Peterson, (2001) suggests that magma ascended through the Virginia Formation via a vertical feeder dike, thereby becoming enriched in sulfides as the Virginia Formation was consumed. The magma then injected into a rift-parallel fault (the NLMD), where high velocity, constrained unidirectional flow prevented the sulfides from precipitating out of the melt. The magma then emptied into the SKI, where the sulfides were eventually deposited along the basal contact. The adjacent BEI is thought to have formed after the emplacement of the SKI, and represents the final magmatic pulse through the Nokomis Deposit.

Rock and paleomagnetic methods were used to characterize the emplacement history and the flow directions within these intrusions. Hysteresis measurements, and petrographic observations indicate that the minerals responsible for the magnetic properties in the rocks are Pseudo-Single Domain (PSD) magnetite, titano-magnetite, and to a much lesser degree, pyrrhotite. The anisotropy of magnetic susceptibility (AMS) indicates that flow within the NLMD was sub-horizontal and unidirectional, parallel to the strike of the dike, and that flow in the SKI was more turbulent and multidirectional. AMS scalar parameters also show that the intrusions formed under dynamic conditions,

with both fluid mechanical and gravitational processes responsible for the formation of mineral foliation.

The characteristic remanent magnetization (ChRM) indicates that NLMD, SKI, and the BEI all formed at roughly the same time, with a small hiatus between the formation of the NLMD and the BEI. Q-values indicate that the local magnetic anomalies are controlled by the natural remanent magnetization, and are not formed due to induction by the current magnetic field.

Table of Contents

List of Figures

List of Tables

I. Introduction

Mineral exploration is an expensive procedure that dominates the budgets of many mining companies. In 2010, Duluth Metals spent 65% ($4,600,000) of total exploration costs on drilling and assay alone (Duluth Metals, Financial Report, Sept. 30th, 2010). Geophysical techniques have the potential to focus mineral exploration efforts and thereby reduce exploration costs. The goal of this study is to apply paleomagnetic techniques so as to better understand the emplacement history of the Nokomis Cu-Ni-PGE Deposit, located within the Duluth Complex of Northern Minnesota. Rock magnetic techniques were used to quantify the magnetic fabric of the rocks and interpret the direction of magma flow within the intrusions, as well as to identify and characterize the grains responsible for the magnetic properties of the rocks. Paleomagnetic techniques were used to determine the geomagnetic recording preserved in the rocks and to interpret the emplacement order of the relative igneous bodies. The Koenigsberger ratio was used to characterize the local magnetic anomalies.

This study had two primary focuses: 1) to study the emplacement history of the Nickel Lake Macrodike (NLMD) and its relationship to the Bald Eagle (BEI) and South Kawishiwi intrusions (SKI). 2) To investigate whether magnetic fabrics, specifically the anisotropy of magnetic susceptibility (AMS), can be used to better locate ore deposits, thereby significantly reducing the exploration costs associated with ore deposits within large igneous intrusions.

Earlier workers have extensively studied the geology of the Duluth Complex. Weiblen (1965) mapped the Bald Eagle Intrusion, and Peterson (2008) mapped the

Nickel Lake Macrodike and the South Kawishiwi,. There have also been several geochronological studies by (Davis and Paces, 1990; Paces and Miller, 1993; Davis and Green, 1997; Hoagland, 2010). Chandler (1990) studied the gravitational and magnetic anomalies. The petrology of the Duluth Complex has been studied by (Weiblen and Morey, 1980; Klewin and Shirley, 1991). Copper-Nickel-PGE mineralization has been studied by (Severson and Hauck, 2003; Miller et al., 1990; Peterson and Albers, 2007; Saini-Eidukat et al., 1989). There have also been several rock and paleomagnetic studies in the Duluth Complex (Tauxe and Kodama, 2009; Maes et al., 2007; Swanson-Hysell et al., 2009). The Geology and Mineral Potential of the Duluth Complex and Related Rocks of NorthEastern Minnesota (Miller, et al., 2002) is a great resource for the scientific history of the Duluth Complex.

II. Background

Magnetism

It is important to first define some of the rudimentary concepts associated with rock and paleomagnetism. Magnetism is produced from electrical currents that form from orbital and spin motions of electrons. According to quantum mechanics, the fundamental unit of magnetism is called the Bohr Magneton (m_b), which is equal to the magnetic moment of a single unpaired orbiting electron. Iron metal, Fe^0, has the following electron configuration: $(1s^2 2s^2 2p^6 3s^2 3p^6) 3d^6 4s^2$. However, in magnetite (Fe_3O_4), Fe has both Fe^{2+} and Fe^{3+}, which have electron configurations of $3d^6 4s^0$ and

$3d^5 4s^0$. Following Pauli's exclusion principle and Hund's rule the spin moments for Fe^{3+} and $Fe2^+$ are 5 and 4 Bohr magnetons, respectively.

There are three basic types of magnetic behaviors: diamagnetism, paramagnetism, and ferromagnetism (See Figure 1). All materials have a diamagnetic component due to the torque of an applied field on the magnetic moment (L), which results in a change in the magnetic moment (ΔL), called Larmor precession. ΔL is always opposite the to direction of the applied field, resulting in a small negative susceptibility. Examples of

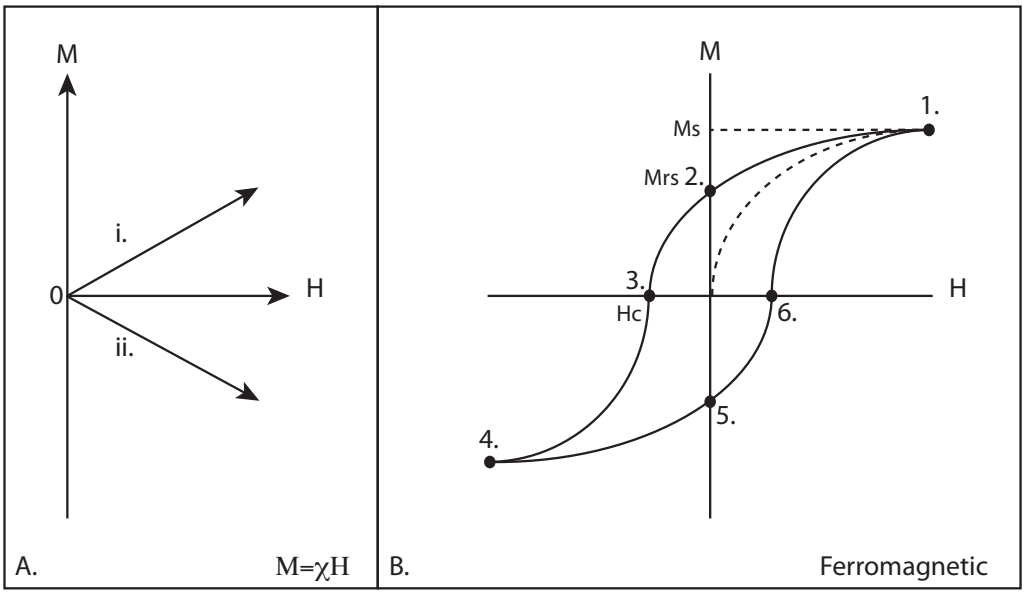

Figure 1: The magnetic response of magnetic materials in an applied field. (A) i. Paramagnetic materials have no spontaneous magnetization in zero field. When a field is applied, the moments will allign in the direction of the applied field creating a positive susceptibility. ii. Diamagnetic materials also have no spontaneous magnetization in zero field. When a field is applied the magnetization is inversly proportional to the inducing field creating a negative susceptibility. (B) Ferromagnetic materials magnetization show a spontaneous magnetization even after the applied field is removed, creating a hysteresis loop where (1.) Saturation magnetization is when all of the magnetic moments are parallel to the applied field. (2.) Magnetic remanence is the amount of magnetization that is retained after the applied field is removed. (3.) The coercivity is the strength of a reversly applied field necessary to remove magnetization. (4), (5), and (6) are equal and opposite to (1), (2), and (3) respectively.

diamagnetic materials include: quartz, calcite, and water.

Paramagnetic materials have electron shells that are partially filled. Randomly oriented electron spins become aligned parallel to an applied field resulting in induced magnetization and a small positive susceptibility. Once the field is removed, the induced magnetization returns to zero. Examples of paramagnetic materials include: olivine, pyroxene, and biotite.

Ferromagnetic materials have incomplete electron shells, but due to the exchange energy between neighboring spins, the magnetization remains after the applied field is removed. These properties can be described with a hysteresis loop. As a ferromagnetic material is subjected to an applied field, the magnetization will slowly increase until saturation magnetization has been reached. This is when all of the magnetic moments in the material are aligned in the direction of the applied field. When the field is removed, the magnetization will begin to drop off until the saturation remanent magnetization has been reached, this is the maximum amount of magnetization the material will "remember". The coercivity is the strength a field applied in the opposite direction necessary to cause the magnetization to equal zero. Examples of ferromagnetic materials include: magnetite, pyrrhotite, and nickel.

As magma cools and magnetic minerals crystalize, the Curie temperature will be reached. This is the temperature at which a ferromagnetic material becomes magnetically ordered, and if the Curie temperature is greater than the blocking temperature remanent magnetization is locked in. When the rock is very hot, the magnetic moments flip around randomly, due the thermal energy as the material begins to cool, the moments will begin

to stabilize. Once the minerals cool below their Curie temperature, the statistical average of all the magnetic moments will be parallel to the direction of the magnetic field at the time of rock formation. If a ferromagnetic material is reheated beyond its Curie temperature, it will act as a paramagnetic material.

There are three basic types of ferromagnetic states: Single Domain (SD), Multidomain (MD), and Pseudo-Single Domain grains (PSD). Single Domain grains have only one magnetic domain, resulting in a grain that is uniformly magnetized in one direction. Due to their high coercivity, the remanent magnetization of SD grains is highly stable. Only very strong induced fields (much greater than the geomagnetic field) are capable of flipping the direction of a SD grain.

In order to reduce magnetostatic energy, large grains develop multiple magnetic domains. Each domain is uniformly magnetization, and may point in a variety of different directions. In contrast, MD grains have a much lower coercivity, and are much less stable than SD grains.

Pseudo-single domain grains are smaller than MD grains and larger than SD grains, but they exhibit characteristics of both. Like SD grains, they carry a high remanence, but like MD they have a low coercivity.

The Earth's Magnetic Field

The Earth's magnetic field is powered by convection in the liquid iron-nickel outer core. This dynamo produces a magnetic field whose time averaged, first order approximation is that of a Geocentric Axial Dipole (GAD). The GAD model looks like a

bar magnet aligned with the rotational axis of the Earth. For the GAD model to be true, the inclination would always be ±90º at the geographic poles, and 0º at the equator. Declination would be 0º everywhere.

The magnetic field can be approximated as a scalar potential field at the Earth's surface, therefore it can be mathematically described using spherical harmonics. After an exhaustive evaluation of the Earth's magnetic field through spherical harmonics, it becomes clear that the field is dominated by the first order terms and that external contributions are very small. The first order terms are geocentric dipoles, whose vector sum is that of a dipole that is currently inclined by 11º to the spin axis (Tauxe, 1998). For more information, the International Geomagnetic Refrence Field (IGRF) can be viewed at the National Geophysical Data Center: http://www.ngdc.noaa.gov.

Perhaps the most important task for a paleomagnetist is to determine what Earth's ancient, or paleomagnetic field was like. This information can help us to understand many geologic phenomena, such as magnetic field reversals and plate tectonics. One way to quantitatively isolate the paleomagnetic field is to use rock demagnetization techniques, such as Alternating Field Demagnetization (AFD) and Thermal Demagnetization.

AFD utilizes a smoothly decaying alternating field to demagnetize a paleomagnetic sample in a field free chamber. As the alternating field is applied to a sample, its magnetic moments will follow along with the field. As the alternating field decays below the coercivity of the sample's magnetic minerals, their magnetization will be locked in. Assuming that there are many grains with a wide range of coercivities in

any given sample, half of the grains with low stability should be locked in one peak field direction, and the other half in the opposite direction, resulting in a net magnetization of zero. This technique is followed around the three orthogonal directions of each sample (Tauxe, 1998).

Thermal energy can also be used to demagnetize a sample. Using stepwise heating and cooling of a sample in a zero field, magnetic grains are progressively unblocked, until all of the natural remanent magnetization has been removed.

Before demagnetizing a sample, its Natural Remanent Magnetization (NRM) is measured. The remaining magnetization is measured after each demagnetization step. The direction of the NRM will change after each step until the Characteristic Remanent Magnetization (ChRM) has been reached. The ChRM is the stable component that is isolated after the removal of the weaker secondary components. The ChRM should plot as a straight line through the origin, on orthogonal end point vector diagrams, from which the declination and inclination of the paleofield can be determined.

The Earth's magnetic field can be approximated as an axial dipole. If we assume a geocentric axial dipole, where inclination is a function of latitude, then the paleolatitude can be calculated with the dipole equation, where I is the inclination, and λ is the co-latitude.

$$(1)\ Tan(I) = 2Tan(\lambda)$$

Frequently the continental configuration has changed since the time that the ChRM was recorded. It is therefore necessary to determine a Virtual Geomagnetic Pole (VGP), is which is the hypothetical geographic location of the paleodipole. Once the VGP and the paleolatitude have been determined, it is possible to reconstruct plate positions, and potentially date the sample.

Geologic Setting

The following is a very brief summary of the Duluth Complex, much of which is found in Miller et al., (2002). Approximately 1100 Ma the Laurentian supercontinent began to rift apart as the result of a mantle plume impinging on the base of the North American craton (Miller et al., 2002). Geophysical data suggests that the Midcontinental

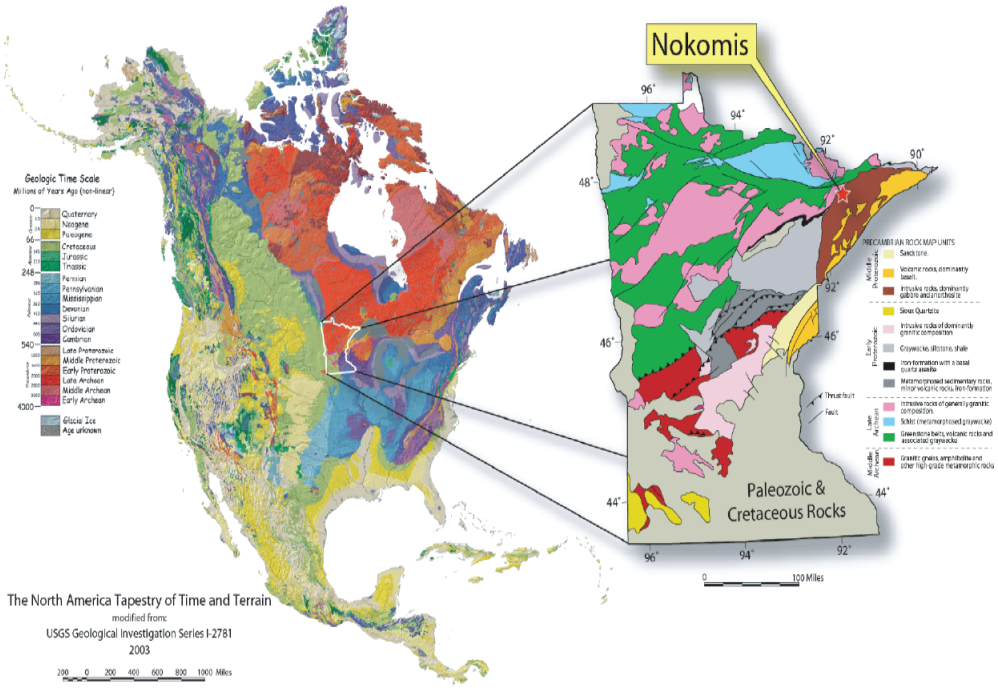

Figure 2: Map showing the location of the study area with respect to Minnesota and North America. Star denotes the Nokomis deposit and field area within the Duluth Complex.

Rift extends 2000 km from its exposure in the Lake Superior region along a segmented, arcuate path from Kansas to Lower Michigan. Seismic data suggests that, in places, the rift consists of 30 km basin infill with volcanics and fluvial sedimentary rocks (Miller et al., 2002). Heat from this plume caused an increase in partial melting of the asthenosphere, producing low viscosity magma that erupted onto the surface creating an enormous volume (1,500,000 km^3) of flood basalts. These volcanic and plutonic rocks make up the Duluth Complex.

The Duluth Complex rocks are sporadically exposed in an arcuate band of 5000 square kilometers, extending from Duluth, North towards Ely (See Figure 2), and east-northeast from Ely toward Hovland, Minnesota. It is one of the largest mafic intrusions in the world, second only to the Bushveld Complex of South Africa. Isotopic data and geochronology suggests that the Duluth Complex formed during four stages: early (1109 to 1107 Ma), latent (1107 to 1102 Ma), main (1102 to 1094), and late (1094 to 1086) magmatic stages (Miller et al., 2002).

The rocks in this study were emplaced during the Main magmatic stage, which is thought to represent the onset of upper crustal separation, as well as the evacuation of the lower crustal magma chambers and continued mantle plume melting. The anorthositc and layered series rocks emplaced at this time are characterized as having a normal magnetic polarity. The anorthositc series rocks are defined as "A structurally complex suite of foliated, but rarely layered, plagioclase-rich gabbroic cumulates." (Miller et al., 2002)

The Layered Series rocks are defined by (Miller et al., 2002) as "A suite of stratiform troctolitc to ferrogabbroic cumulates that compromises at least 11 variably differentiated mafic layered intrusions and occurs mostly along the base of the Duluth Complex." Most of these rocks dip to the SE toward the rift axis and were emplaced between the Anorthositic series and pre-Keweenawan rocks. Anorthositic rocks are often found as inclusions within the Layered Series, but never the reverse. This study focuses on three intrusions associated with the Layered Series intrusions: NLMD, SKI, and the BEI (see Figure 3).

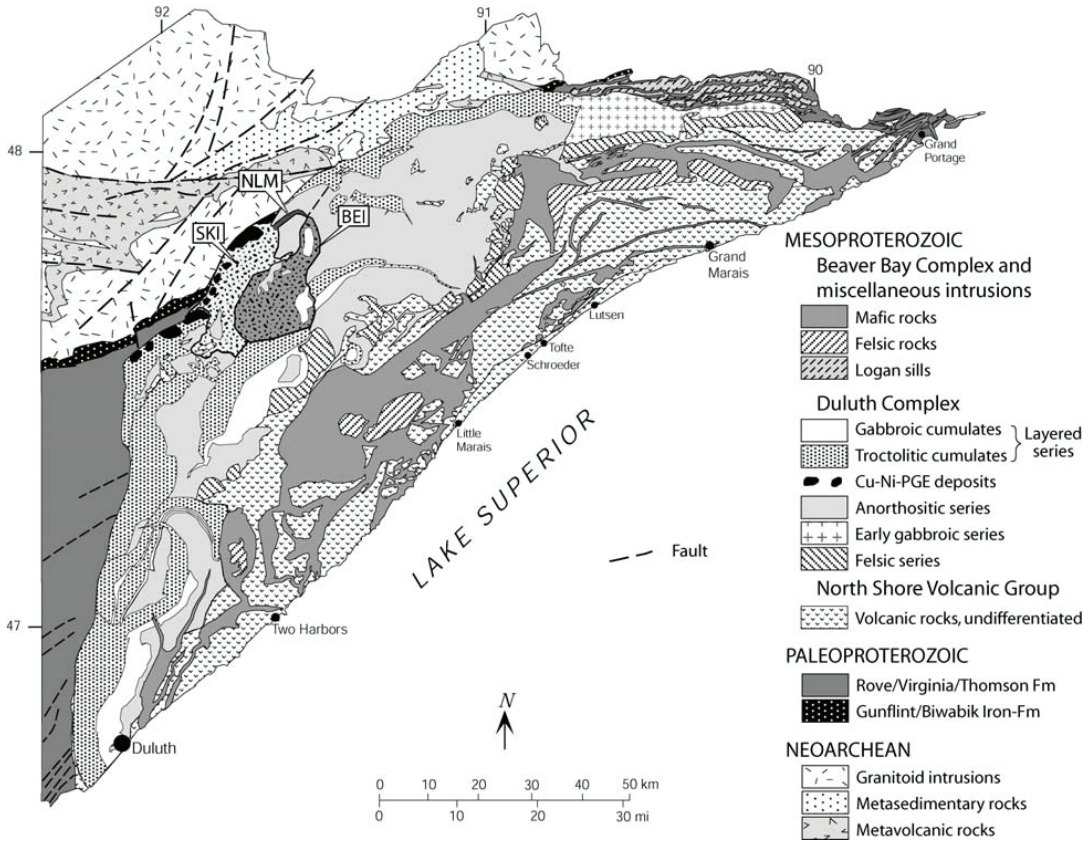

Figure 3: Location of the Bald Eagle Intrusion (BEI), Nickel Lake Macrodike (NLMD), and the Bald Eagle Intrusion (BEI) with respect to the greater Duluth Complex. (From Miller et al., 2002)

It has long been known that northern Minnesota has the potential to be a global player in the mining and development of precious metals. Previously, the value of such materials did not support the cost for exploration and development.

One such resource is the Nokomis Deposit, which is located in northeastern Minnesota, southwest of the town of Ely (see Figure 1). On a contained metals basis, it is one of the largest precious metal resources in the world. A 2009 resource estimate indicated that Nokomis Deposit contains at least 550 million tons of mineral resources (see Figure 4).

NOKOMIS DEPOSIT* TOTAL CONTAINED METAL**		
Metal	Indicated	Inferred
Copper	7.75 Billion lbs.	3.82 Billion lbs.
Nickel	2.43 Billion lbs.	1.25 Billion lbs.
Cobalt	121.26 Million lbs.	60.37 Million lbs.
Platinum	3.11 Million ozs.	1.63 Million ozs.
Palladium	6.93 Million ozs.	3.60 Million ozs.
Gold	1.63 Million ozs.	0.80 Million ozs.
TPM (Pt+Pd+Au)	11.67 Million ozs.	6.03 Million ozs.
Silver	37.42 Million ozs.	18.10 Million ozs.

* Does not include the newly acquired resources from Franconia Minerals.

** Based on December 10, 2009, Technical Report On The Mineral Resource Estimate For The Nokomis Deposit On The Nokomis Property, Minnesota, U.S.A. For complete resource details, see page 10 of this Report.

Figure 4: Total contained metal in the Nokomis Deposit as of Dec 10, 2009. From the Duluth Metals Annual Report 2010.

Bald Eagle Intrusion

The BEI is an approximately 16 by 5 km, layered intrusion located along the northwestern margin of the Duluth Complex. It was emplaced amongst the SKI, Greenwood Lake Intrusion (GLI) and the Anorthositic Series country rock. Structural data collected by (Weiblen, 1965) suggests that the intrusion is funnel shaped with steep foliation and layering in the northern portion of the Bald Eagle Intrusion. The funnel is defined by concentrically dipping foliation, which gradually decreases from nearly 90 degrees on the northwestern margin of the intrusion, to horizontal at Tonic Lake, located near the North-Central portion of the intrusion. This structural data, along with gravitational anomalies at the Northern margin of the intrusion, suggests that the funnel necks down to a steep feeder (Miller and Severson, 2002).

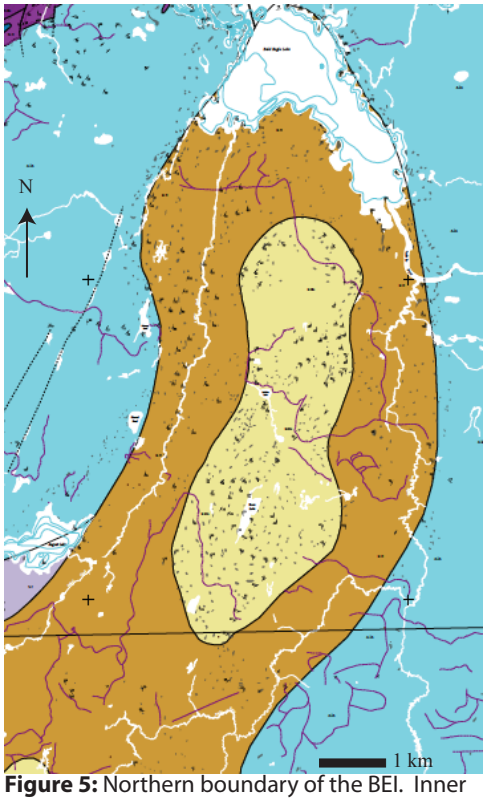

Figure 5: Northern boundary of the BEI. Inner yellow ring is the Bald Eagle Gabbro (B-oG). Outer brown ring is the Bald Eagle Troctolite (B-T)

The intrusion consists of two major rock units: Olivine gabbro (B-oG), and Layered troctolite (B-Tl). The B-oG defines the inner core of the BEI and consists of medium-grained, well-foliated, oxide-bearing olivine gabbro. The outer core is defined by the B-T phase, which consists of dark green, medium-grained, steeply dipping, well-foliated, modally layered troctolite to melatroctolite (Peterson, 2008). Each unit contains

less than 1% of interstitial Fe-Ti oxides. There is a gradational contact between the outer ring of troctolite and the inner ring of gabbro. This contact is a zone of approximately 100 meters wide as is distinctly marked by an increase in pyroxene content.

Due to the upright funnel shape and depth of erosion, any upper differentiates that may have existed have been destroyed (Miller and Severson, 2002). Weiblen and Morey (1980) interpreted the structural habit and the adcumulate nature of the BEI to be an indication of an open conduit to higher intrusions, and perhaps volcanic flows (Miller and Severson, 2002).

Miller and Severson (2002) outline a model suggesting that the BEI and the SKI may have been emplaced by the successive overplating of magmas from a common feeder dike. This feeder dike originates from beneath the northern portion of the BEI, just north of Bald Eagle Lake it arcs works its way along the trace of the NLMD. This model suggests that the BEI was formed well after the SKI, and had a much more complete cumulate sequence than is preserved. (Miller et al., 2002).

Nickel Lake Macrodike

Located within a major rift-parallel normal fault that trends toward the southwest, the NLMD (see Figure 6) is a steeply dipping troctolitic and gabbroic intrusion, which is approximately 5 by 1 km (Peterson, 2008). The deep erosion of the neighboring BEI has led to the interpretation that there is a regional tilt toward the South where the margin of NLMD is structurally higher than the northern margin. The NLMD has been interpreted by (Peterson, 2008) as a feeder dike to the SKI. Peterson 2008 further interprets the

structurally higher northern region as the location where the magma changed from dike-like to sill-like, as it entered the expanding magma chamber associated with the SKI.

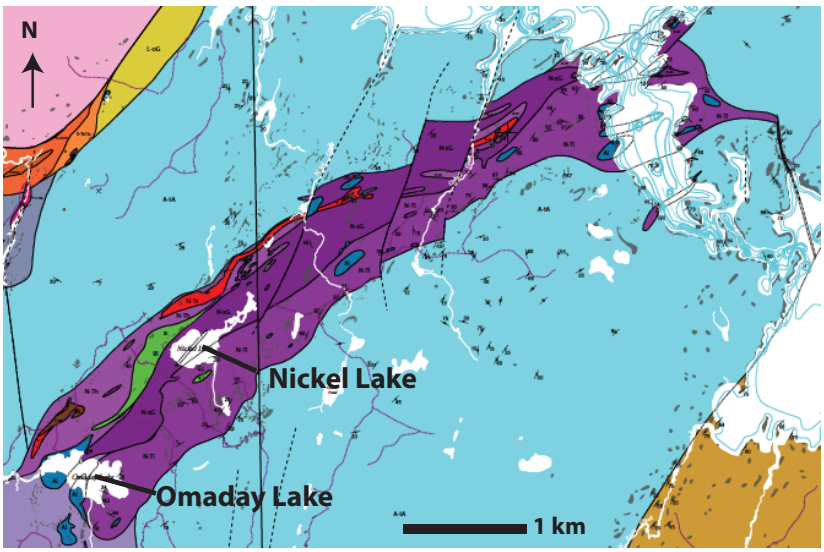

Figure 6: The Nickel Lake Macrodike. Light Purple unit on the East is the Nickel Lake Oxide Gabbro (N-xG), Dark Purple in the middle is the Layered Troctolite (N-Tl), and the light purple on the West is the heterogeneous Troctolite (N-TH).

Rocks types associated with the NLMD include: Oxide gabbro (N-xG), Layered troctolite to dunite (N-Tl), Heterogeneous troctolite (N-Th), and Sulfide-bearing troctolite (N-Ts). The N-xG phase is composed of dark-grey, coarse-grained to pegmatitic olivine-gabbro to melagabbro. These rocks contain magnetite and ilmenite, making them potentially useful for paleomagnetic studies. Inclusions of other rock types, along with crosscutting relationships within the dike have led to the interpretation that N-xG is the youngest phase in NLMD (Peterson, 2008).

The N-Tl phase is composed of grey to black, medium-grained, well-layered troctolite, melatroctolite, and dunite. Lamination of plagioclase and olivine parallel to modal layering is commonly observed, as well as igneous scours and crossbedding. Layering possibly developed as the up-welling magma streamed through the expanding feeder dike (Peterson, 2008).

The N-Th phase is composed of light to dark grey, medium to coarse-grained, inclusion-rich heterogeneous troctolitic rocks. This unit is composed of intermixed troctolite, anorthositic-troctolite, melatroctolite, and gabbroic phases surrounding numerous anothositic country rock xenoliths. Inclusions in this unit, such as the Bibwaki Iron Formation, are aligned parallel to the NLMD. This phase is interpreted to be the initial highly dynamic magmatic phase of the dike that carried exotic inclusions from deep in the crust to their present level (Peterson, 2008).

The N-Ts Phase is composed of a, medium to coarse-grained, sulfide-bearing heterogeneous troctolitic and gabbroic rocks. The sulfides in these rocks make them more susceptible to weathering processes than it's non-sulfide bearing counterparts.

South Kawishiwi Intrusion

The SKI is an 8 by 32 km arcuate band, composed mainly of plagioclase and olivine troctolite, the SKI defines the NE margin of the Layered Series of the Duluth Complex. The footwall to the SKI is most often the Anorthositic Series, although occasionally the intrusion is in direct contact with the Virginia Formation, the GRB, and the Biwabik Iron Formation. Xenoliths of these footwall rocks, along with some basaltic hornfels from the North Shore Volcanic Group, were entrained within the intrusion during its emplacement and can be observed in outcrop (Peterson, 2001).

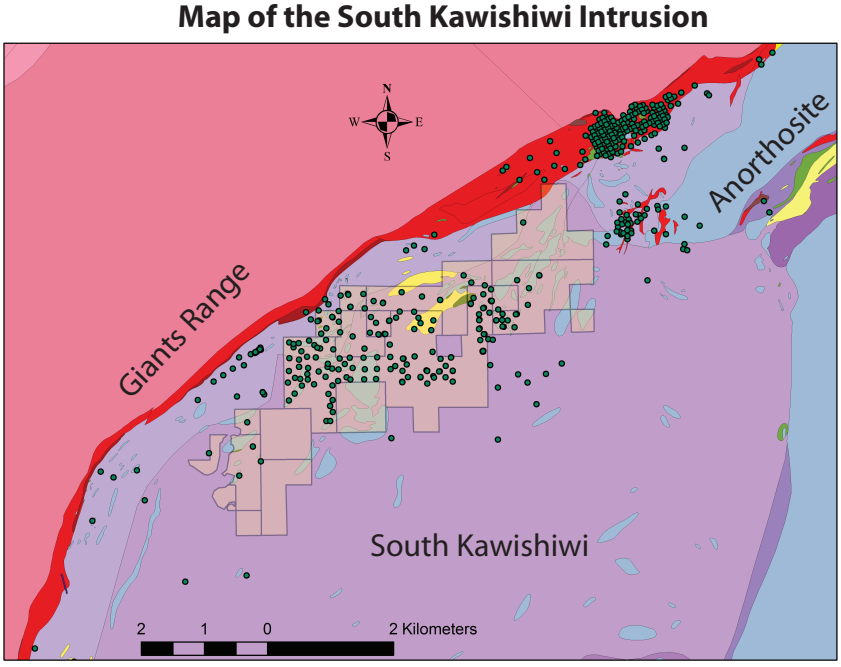

Figure 7: Map of the SKI. Pink rocks are the Giants Range Batholith (GRB), blue is the Anorthositic Series, purple is the SKI, and red is the mineralized zone. Shaded area is the Nokomis Deposit, and the green circles indicate the location of exploration boreholes.

The Nokomis Deposit, and other related mineral deposits found in and near the SKI, along the basal contact of the Layered Series are some of the largest untapped Cu and PGE ore deposits in North America. The genesis of these ores and other rocks associated with the SKI intrusion are interpreted by Peterson (2008) to have been deposited during three separate magmatic phases. These phases in order of occurrence are: (1) Open Style Injection, (2) Confined Style Injection, and (3) Main Magmatic Injection.

During Stage 1, crystal-laden slurries of troctolitic melt were injected into the initial magma chamber of the SKI. The crystals in this slurry were xenocrysts derived from footwall rock, such as the Anorthositic Series, the Virginia Formation, the GRB, the Biwabik Iron Formation, and the North Shore Volcanic Groups basalts. The melt also hosted sulfide-bearing liquid droplets. Metals were poorly partitioned during Stage 1, due to limited turbulent flow (Peterson, 2008), and rock types formed during this stage

include sulfide-bearing, heterogeneous troctolitic rocks (S-Ts1), sulfide-poor, heterogeneous troctolitic and gabbroic rocks (S-Ts1b), sulfide-bearing melatroctolite (S-mTs1), and augite-bearing troctolite (S-pT1). S-pT1 is interpreted by (Peterson, 2008) to have formed in the upper liquid portion of the magmatic slurry. Structurally-controlled, sulfide-bearing, PGE-rich, troctolitic rocks (S-Ts4), and structurally-controlled, sulfide-bearing troctolite and anorthosite (S-Ts3) were also formed during Stage 1, but are interpreted by Peterson, 2008 to have been formed in relation to hydrothermal deposits and sulfide injections occurring thousands of feet above the SKI basal contact.

During Stage 2, crystal-laden slurries of troctolitic melt were once again injected into SKI. Turbulent flow mixed this slurry with the basal magmatic slurry allowing for the further partitioning of metals into the sulfide fraction (Peterson, 2008). Rock types formed during Stage 2 include sulfide-bearing, noritic rocks (S-Ns), sulfide-bearing troctolitic rocks (S-Ts2), sulfide-bearing melatroctolite (S-mTs2), pegmatitic troctolitic rocks (S-Tpeg), and augite-bearing troctolite (S-pT2). S-pT2 is interpreted by Peterson, 2008 to have formed in the upper liquid portion of the magmatic slurry.

During Stage 3, magma rich in plagioclase and olivine phenocrysts was injected into the growing SKI magma chamber (Peterson, 2008). Rocks formed during this phase include anorthositic troctolite to troctolite (S-aT-T), and troctolite to anorthositic troctolite (S-T).

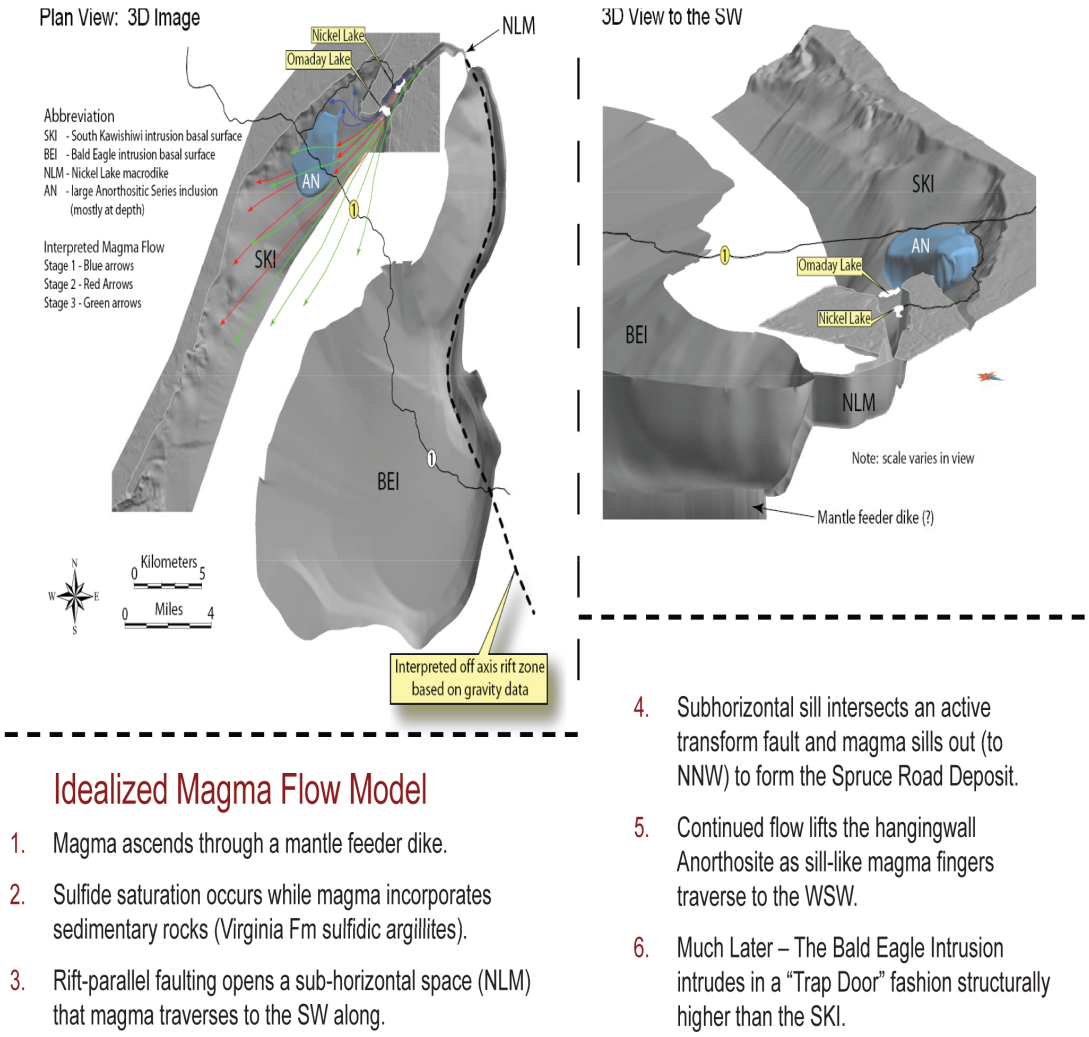

Idealized Magma Flow Model

1. Magma ascends through a mantle feeder dike.
2. Sulfide saturation occurs while magma incorporates sedimentary rocks (Virginia Fm sulfidic argillites).
3. Rift-parallel faulting opens a sub-horizontal space (NLM) that magma traverses to the SW along.
4. Subhorizontal sill intersects an active transform fault and magma sills out (to NNW) to form the Spruce Road Deposit.
5. Continued flow lifts the hangingwall Anorthosite as sill-like magma fingers traverse to the WSW.
6. Much Later – The Bald Eagle Intrusion intrudes in a "Trap Door" fashion structurally higher than the SKI.

Figure 8: Regional magma flow model from Peterson, (2001)

The model described by Peterson, (2001) is illustrated in Figure 8, and describes the emplacement of the Nokomis Deposit. Magma first rises through a vertical conduit, which was located beneath the current location of the BEI. This magma became enriched in sulfides as it melts the Virginia Formation. This magma then moves toward the NLMD, where constrained, unidirectional flow, and high velocity conditions prevents the bulk of the sulfides from precipitating out of solution. Upon exiting the NLMD, flow within the SKI becomes multi-directional and the sulfides precipitate out of solution

along the basal contact of the SKI intrusion. Finally, the BEI is emplaced in a trap door fashion along the feeder dike.

This study used AMS to verify that within the NLMD, there was subhorizontal flow parallel to the strike of the macrodike, and that flow directions within the SKI are multi-directional, but averaging toward the northwest direction, toward the Nokomis Deposit. By successfully verifying this model, this research demonstrated that rock and paleomagnetic techniques can be useful tools in the mineral exploration industry.

IV. Methods

Sample Collection and Preparation

Paleomagnetic cores were collected using a gas powered drill and oriented with both a sun and magnetic compass. 12 sites were sampled within the NLMD, 12 within the SKI, and 8 from the BEI. Each site produced an average of 5 cores. Each core was subdivided into up to 4 samples, 25 mm in diameter and 22 mm in length, for a total of 345 samples.

Anisotropy of Magnetic Susceptibility

The behavior of particles in viscous fluids has been studied intensely over the last century. The subject's roots can be traced back to Einstein's PhD dissertation on Brownian motion (Einstein, 1906). Einstein's equations considered the motion of spherical particles and were eventually extended to ellipsoidal grains (Jeffery, 1922). Jeffery hypothesized that both prolate and oblate grains in a laminar fluid should be oriented such that their long axes are parallel to the direction of flow. The extent of the

resulting shape preferred orientation (SPO) causes a rock's physical properties to become directionally dependent, or 'anisotropic'. For example, the shape preferred orientation of olivine grains in rocks near subduction zones can cause seismic waves to travel faster in one direction than another. Measurements of the AMS utilize the shape-preferred orientation (SPO) and lattice preferred orientation (LPO) of magnetic grains to interpret the mineral fabrics of igneous intrusions (Borradaile & Jackson, 2004).

AMS measurements in this study were collected using an AGICO Kappabridge, which operates using a 300 A/m AC field with a frequency of 920 Hz. Samples were measured using the 15 position rotational scheme outlined by Hext (1963). An isotropic sample with no shape preferred orientation would yield identical magnetic susceptibility values regardless of the sample's orientation. Deviations from this idealized behavior are represented using a second rank tensor (Jel´ınek, 1978; Tarling and Hrouda, 1993).

(2) $M = K_{ij}H$

(3) $$k_{ij} = \begin{vmatrix} k_{11} & k_{12} & k_{13} \\ k_{21} & k_{22} & k_{23} \\ k_{31} & k_{32} & k_{33} \end{vmatrix}$$

The tensor in equation (3) can be used to represent an ellipsoid whose principle axes are given by the eigenvectors of the susceptibility tensor, k_{max}, k_{int}, and k_{min}. The length

of each principle axes is given by the corresponding eigenvalue τ_{max}, τ_{int}, and τ_{min}. There are several parameters that come out of the tensor in (2) which can be used to determine the shape of the AMS ellipsoid. The shapes can range from prolate (4) to triaxial (5) to oblate (6), (Tauxe, 1998).

(3) $\tau_{max} > \tau_{int} \approx \tau_{min}$

(4) $\tau_{max} > \tau_{int} / > \tau_{min}$

(5) $\tau_{max} \approx \tau_{int} > \tau_{min}$

Several studies have developed methods to characterize magnetic fabrics, e.g., Aziz-ur-Rahman et al. (1975), Hrouda (1982). However, Jel´ınek, (1981) determined the most widely used method to quantify AMS parameters, specifically the degree of anisotropy (P_j), and the shape factor (T).

(6) $$p_j = \exp(2[\left(\ln\tau_1 - \ln(\tau_1+\tau_2+\tau_3)^{1/3}\right)^2 + \left(\ln\tau_2 - \ln(\tau_1+\tau_2+\tau_3)^{1/3}\right)^2 + \left(\ln\tau_3 - \ln(\tau_1+\tau_2+\tau_3)^{1/3}\right)^2]^{1/2})$$

(7) $$T = \left[2\ln(\tau_2/\tau_3)/\ln(\tau_1/\tau_3)\right] - 1$$

The degree of anisotropy is useful in determining the intensity of anisotropy in a sample. The shape factor is important because it provides insight into the geological

process that produced the anisotropy. For example, most undisturbed sediments yield oblate magnetic fabrics ($T > 0$), whereas sediments affected by slumping display prolate magnetic fabrics ($T < 0$) (Schwer and Tauxe, 2003). The "Jelinek plot" displays P_j versus T and is commonly used by the rock magnetic community to quickly characterize the shape of an AMS ellipsoid.

AMS is frequently used to determine the flow direction in igneous intrusions such as mafic dikes, sills, laccoliths and cone sheets (Knight and Walker, 1988; Ernst and Baragar 1992; Ferré et al., 2002; O'Driscoll et al., 2006). These earlier studies show that AMS ellipsoids in intrusive igneous rocks are usually oriented such that K_{max} is parallel (to subparallel) to the direction of magma flow and K_{min} is perpendicular to the flow direction. Because magma flow can occur along the positive or negative direction of K_{max}, additional knowledge of the intrusion and its environment is frequently required to establish the absolute direction of flow. A study by (Knight and Walker, 1988) determined the absolute flow direction in a mafic dike by observing the imbrication of K_{max} directions from successive samples collected along the dike's margins.

Some AMS studies produce results that do not consistently show K_{max} parallel to the direction of flow. Instead, these studies display "inverse magnetic fabrics", where K_{min} is parallel to the flow direction and K_{max} is perpendicular to the direction of flow. This phenomenon occurs in samples dominated by elongate grains of single-domain magnetite. Because the magnetization in such grains is controlled by shape anisotropy, the direction of maximum susceptibility for an elongate grain of single domain magnetite is perpendicular to its long axis. As a result, the K_{max} direction for such samples will be

oriented perpendicular to the direction of flow. Such samples can be identified by their low bulk susceptibility and by elevated coercivities. In order to properly interpret the geologic processes that produced a rock's magnetic fabric, great care must be taken to identify such inverse fabrics (Rochette et al., 1999; Ferré, 2002).

Tilt Correction

It is possible that the paleomagnetic recording preserved within the Duluth Complex, and its corresponding magnetic fabrics has been tilted toward the SE as a consequence of the intense gravity high associated with the cool, Dense rocks of the Midcontinental Rift. The average strike and dip of the nearby North Shore Volcanics is 045º and 25º S respectively, which we used as a maximum potential tilt correction. Getting an accurate sense of the amount of regional dip from within the field area is not realistically feasible, so we present our results as two end members: non-tilt-corrected and tilt corrected data.

Magnetic Mineralogy

Strong-field thermomagnetic curves were used to measure the temperature dependence of saturation magnetization in four samples from each of the three intrusions. Experiments were conducted using a Princeton Measurements vibrating sample magnetometer. Samples were suspended in a continuous stream of helium gas to prevent oxidation, and exposed to a constant 1 T magnetic field, while being slowly heated from 25°C to 700°C. Samples were then allowed to cool back to 25°C under the same conditions. Measurements of the sample's saturation magnetization were collected

during heating (red) and cooling (blue). The Curie temperatures of magnetic minerals within each sample were identified using inflection points in the thermomagnetic curve collected during heating. The exact value of these inflection points was determined using three methods: The Moskowitz technique (Moskowitz, 1981), the second derivative method (Tauxe, 1998), and the intersecting tangents technique (Grommé et al., 1969). Hysteresis loops and backfield curves were measured before and after each strong-field thermomagnetic experiment. These measurements produce the bulk parameters necessary to construct Day plots, which are frequently used to estimate the magnetic grain size distribution within a sample (Dunlop, 2002).

Paleomagnetic Characterization

In order to obtain each sample's NRM ChRM, both AFD and thermal demagnetization techniques were employed. The AFD study used a 2G Enterpises cryogenic magnetometer with the following AF sequence (in mT): NRM, 15, 18, 21, 24, 27, 30, 33, 36, 45, 55, 70, 80, 100, 130, 160. The data was then displayed with equal area steronets, and Zijderveld plots after (Zijderveld, 1967) using the software PaleoMag X.

During thermal demagnetization, the following heating steps were used: 25º, 125º, 200º, 275º, 325º, 350º, 455º, 525º, 550º, 580º, and 610º. To further classify the magnetic mineralogy, the susceptibilities of each sample were measured using the Kappa Bridge following each heating step.

Q-Values

Rocks typically carry an induced (J_i) and a remanent magnetization (J_r). The induced magnetization is the samples bulk magnetic susceptibility times the Earth's magnetic field, and is parallel to the current geomagnetic field, which is 56.95 μT at our field site. The remanent magnetization is parallel to the Earth's field at the time magnetization was acquired. The Koenigsberger ratio, or "Q" (Koenigsberger, 1938), is the ratio of the natural remanent magnetization to induced remanent magnetization and can help characterize local magnetic anomalies.

$$(8)\ Q = \frac{J_r}{J_i} \quad \text{Or} \quad Q = \frac{J_r}{\chi * H_e}$$

Where J_r is the NRM, J_i is the induced magnetization, χ is susceptibility and H_e is the Earth's present magnetic field.

Rocks with Q-values less than 1 have remanence that is dominated by induced magnetization and should therefore be associated with positive magnetic anomalies. Likewise, rocks with Q-values greater than 1 have a remanence dominated magnetization. The remanence may be in any direction other than the modern field direction, and may even display a reversed or negative magnetic anomaly. Chandler (1990) found that the Q-values of Duluth Complex rocks is typically greater that 1, indicating that remanence dominates the magnetic signature with an average NRM direction of 290°/40º.

V. Results

Magnetic Mineralogy

Thermomagnetic results from select samples from each intrusion are shown in Figure 9-11 below. The induced magnetization that is measured during these experiments is sum of all paramagnetic, diamagnetic, and ferromagnetic materials in the rock sample. In most samples from the study area the paramagnetic signal comes from minerals such as olivine and pyroxene, and the diamagnetic susceptibility from minerals such as plagioclase and quartz. Both of these components are minor, relative to the strength of the ferromagnetic signal. As the temperature increases, we observe sudden decreases in the induced magnetization that are characteristic of the Curie temperatures for specific ferromagnetic minerals found within the sample. Increases in the induced magnetization that are observed on heating are typically interpreted the formation of new ferromagnetic minerals.

Thermomagnetic data from BEI samples are shown in Figure 9A and B. These graphs provide evidence for low-Ti titanomagnetite with Curie temperature estimates ranging from 574 to 578˚C (Figure 5A) and 563 to 584˚C (Figure 9B). Sample BE0303C (Figure 9A) is highly reversible, whereas sample BE0306C (Figure 9B) shows evidence for the loss of ferromagnetic material during cooling. The heating data in Figure 9B also shows evidence of a second magnetic mineral phase with a Curie temperature estimate of approximately 325˚C (possibly pyrrhotite), which is not evident on cooling.

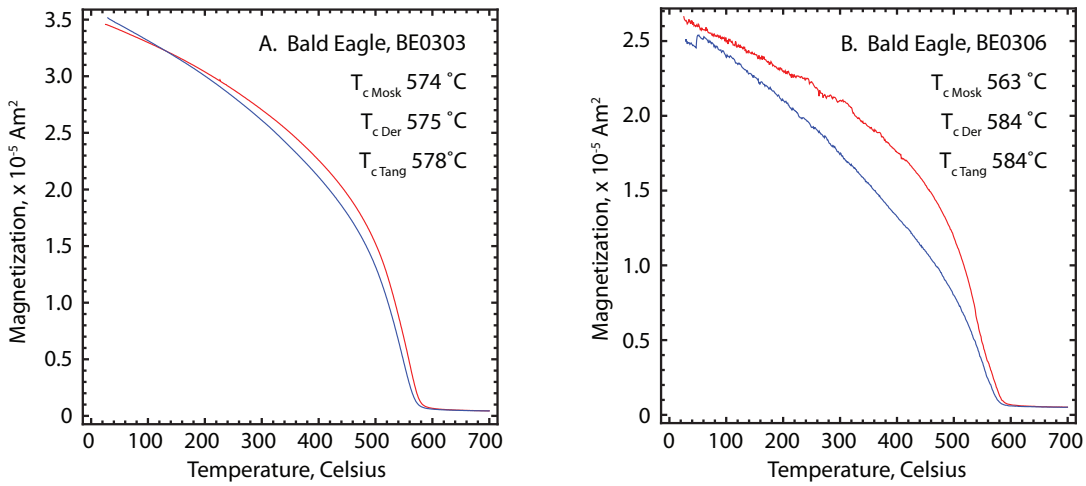

Figure 9: Thermomagnetic curves for Bald Eagle Intrusion (a, b). Red (blue) lines indicate the induced magnetization during heating (cooling).

The NLMD samples are illustrated in Figures 10A through D. All samples display irreversible behavior, and some show evidence of multiple carriers of magnetic remanence. Once again, these graphs provide evidence for low-Ti titanomagnetite with Curie temperature estimates ranging from 553 to 561˚C, (Figure 10A), 559 and 564°C (Figure 10B), 551 to 605°C (Figure 10C), and 551 to 561°C (Figure 10D). Sample NLMD_NGX_010202C (Figure 10D) contains a second ferromagnetic phase with an estimated T_C of 325^{0}C, which may be interpreted as pyrrhotite.

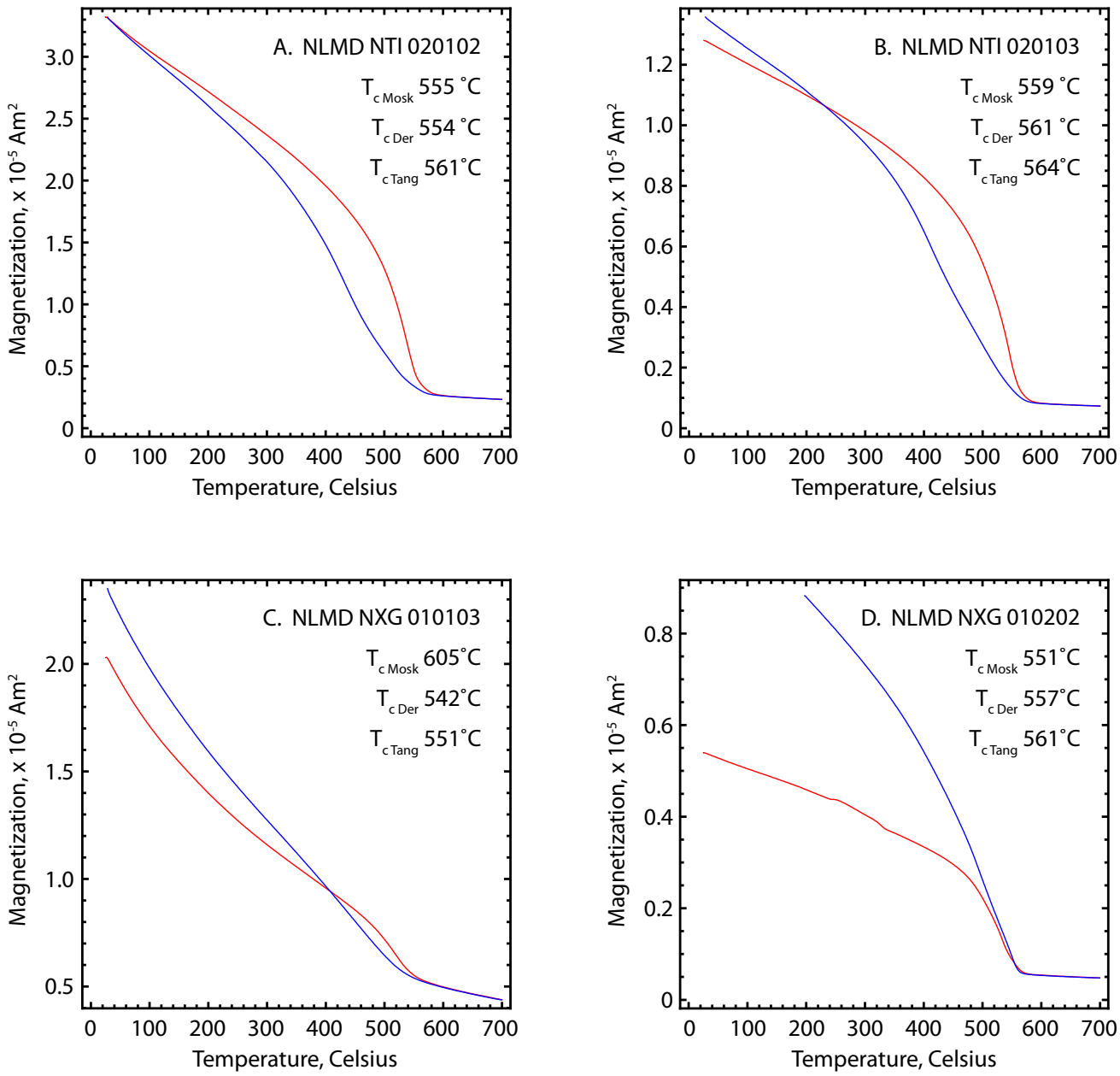

Figure 10: Thermomagnetic curves for Nickel Lake Macrodike. Red (blue) lines indicate the induced magnetization during heating (cooling).

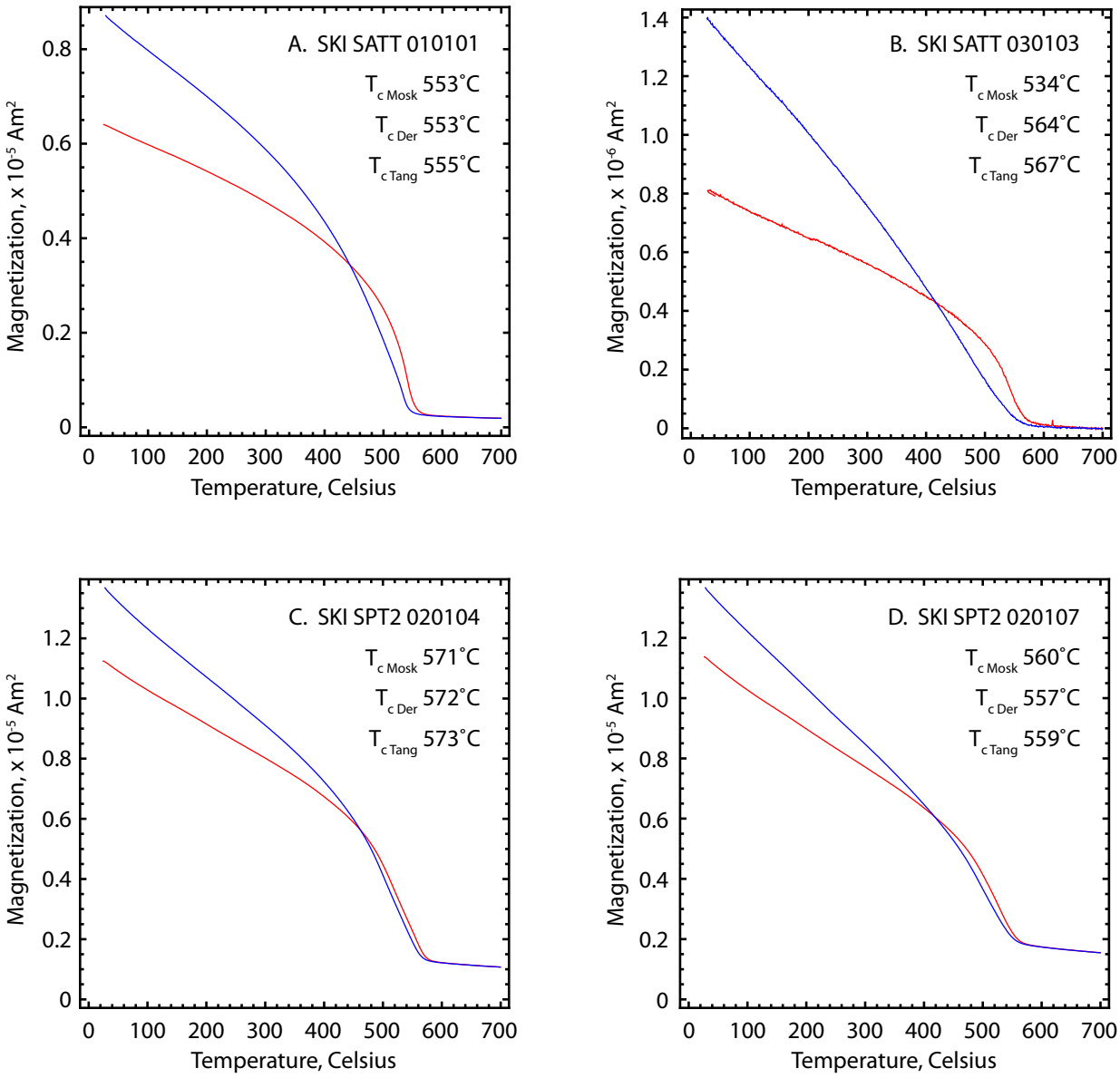

Figure 11: Thermomagnetic curves for the South Kawashiwi Intrusion. Red (blue) lines indicate the induced magnetization during heating (cooling).

The thermomagnetic results from the SKI shown in figures 11 A through D. All samples display irreversible behavior, and some show evidence of multiple carriers of magnetic remanence. Once again, these graphs provide evidence for low-Ti magnetite with Curie temperatures ranging from 553 to 555ºC (Figure 11A), 534 to 567ºC (Figure 11B), 571 to 574ºC (Figure 11C), and 559 to 560ºC (Figure 11D). Sample SKI_SATT_010101C (figure 11B) contains a second ferromagnetic phase with an estimated T_C of 325ºC, which may be interpreted as pyrrhotite.

In order to monitor the stability of the magnetic mineral assemblages and glean more information about its original composition, we measured the room temperature susceptibility after each demagnetization step. This was using the Magnon VFSM Susceptibility Bridge. This approach allows us to monitor when magnetic mineral phases are either destroyed, or transformed into another more stable phase, such as magnetite.

The susceptibility data from all three intrusions is shown in Figure 12 and there is relatively little change in susceptibility from room temperature up to about 440°C. After the 440°, step the susceptibilities either decrease or increase dramatically, it is rare to remain unchanged. The increase in susceptibility is likely due to the transformation of sulfides, such as pyrite and pyrrhotite, into magnetite. A decrease in susceptibility indicates that the magnetic phases have been destroyed, or oxidized into less magnetic minerals, such as hematite.

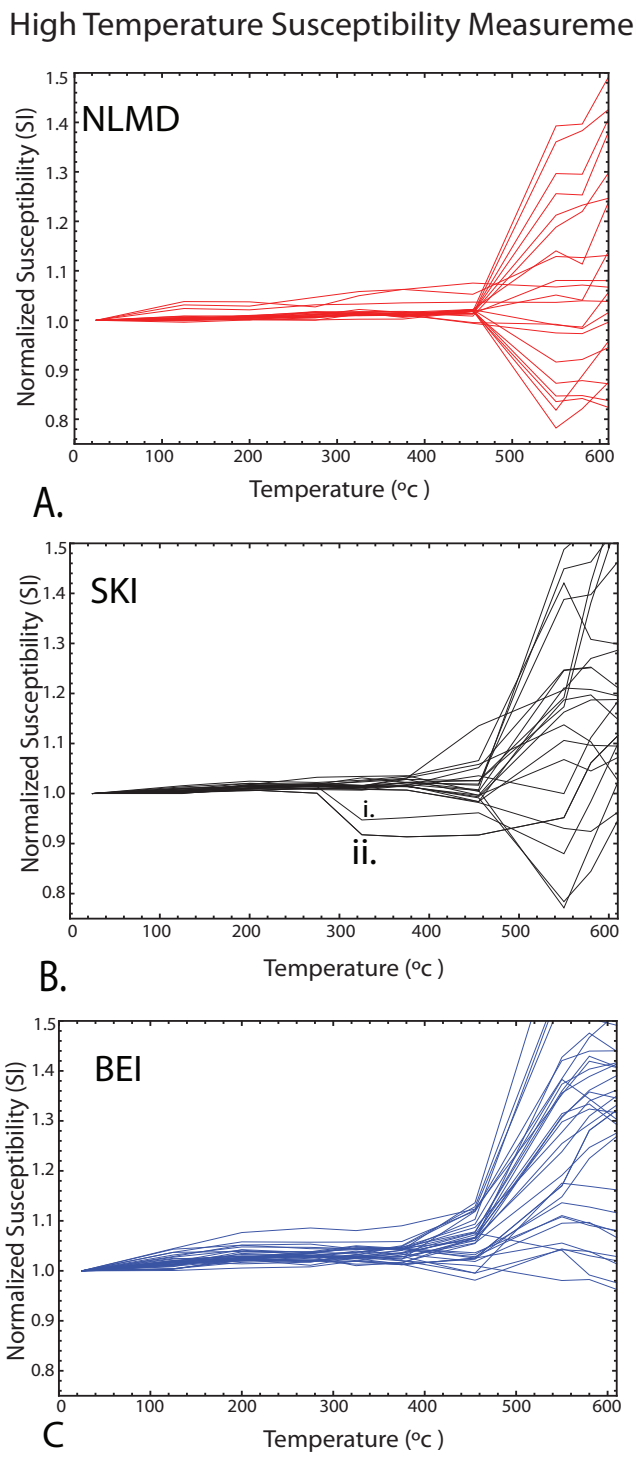

Figure 12: Temperature vs susceptibility for the NLMD (A), SKI (B), and BEI (C). The increase in susceptibility after ~440° suggests the transformation of sulfides into magnetite. A decrease in susceptibility indicates that a magnetic phase has been destroyed or converted to a less magnetic minerals such as hematite. Points i. and ii. in the SKI (B) indicate the destruction of pyrrhotite at a temperature of 320°.

Even more information about the magnetic carriers can be determined by comparing the thermomagnetic data to the susceptibility data. In the thermomagnetic data, select samples from all three intrusions displayed the Curie temperature for pyrrhotite around 320°. The susceptibility data for the SKI shows two samples with decreasing susceptibility around the same temperature (Figure 12B, i. and ii), suggesting that pyrrhotite has been destroyed after heating. However, the BEI and NLMD pyrrhotite suggested by the thermomagnetic data in figure 9B are not evident in the susceptibility data (Figure 12C). This indicates that pyrrhotite is not pervasive in all rock types, and that in these cases the increase in susceptibility at 440ºC is likely due to the production of magnetite via the alteration of pyrite.

Reversible curves observed in the thermomagnetic measurements such as BE0303 in Figure 9A are also observed in the susceptibility data where there is almost no change in the susceptibility across the entire range of temperatures. Likewise, thermomagnetic data whose cooling curves are much greater than the heating curves (Figures 11B and 10D) due to the formation of ferromagnetic minerals is also observed in the susceptibility data where there are drastic increases in susceptibilities upon heating.

Grain Size Characterization

In order to characterize the magnetic grain sizes in each of the intrusions, hysteresis loops and backfield curves were collected before and after each thermomagnetic measurements.

The hysteresis parameters for all measured samples have been plotted on a Day plot (Dunlop, 2002), which plots the ratio of the magnetic remanence and saturation

magnetization (M_r/M_{rs}) against the ratio of remanent force against coercive force (H_{cr}/H_c). The Day plot is divided into sections, which help identify weather the bulk magnetic mineral assemblage is magnetite is SD, MD, or PSD.

Results shown in Figure 13 suggest that the magnetic grain sizes can be classified as being predominantly PSD, or a mixture of SD and PSD grains. PSD grains are the result of high remanence similar to SD grains and low coercivity similar to MD grains. In magnetite, PSD grains typically occur around 0.1-20 μm, for pyrrhotite this occurs between 2-3 and 40μ, (Dekkers, 1988).

Understanding the grain size is important in characterizing magnetic fabrics using techniques such as AMS, because SD behavior can result in inverse fabrics. It is

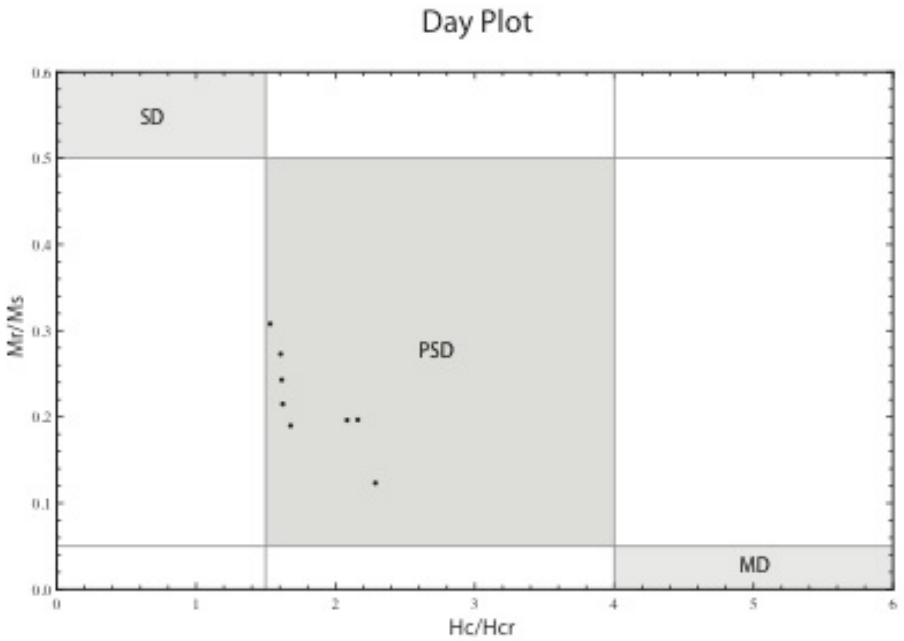

Figure 13: The Day Plot, after Day et al., (1977) is often used to determine magnetic grain size (Mr is the remanent magnetization; Ms is saturation magnetization; Hc is remanent magnetic coercivity; Hcr is the remanent magnetic coercivity). All samples plot within the range of pseudo-single domain grains (PSD).

important to note that such hysteresis measurements are bulk averages, and that each sample has a continuum of grain sizes.

Magnetic Fabric

Analysis of AMS Scalar Parameters

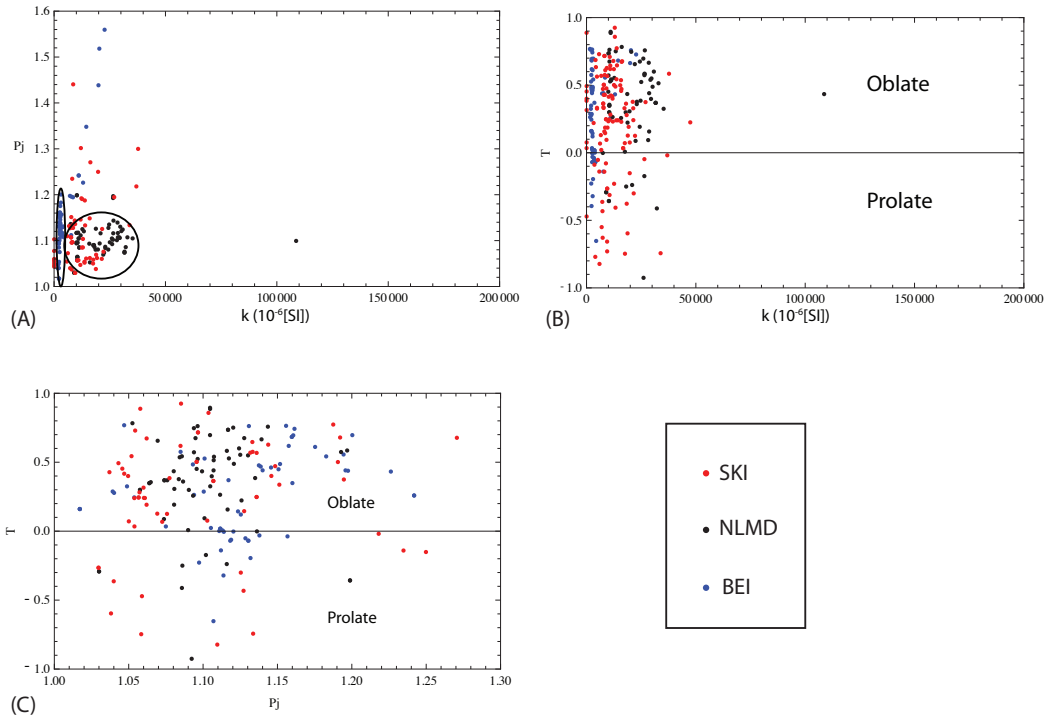

Figure 14: Scalar AMS parameters for the BEI (Blue), NLMD (Black), and the SKI (Red). (A) Degree of anisotropy (P_j) vs. susceptibility (k). The BEI has a relativly small range of susceptibilites and relativly large range in the degree of anisotropy. (B) Shape factor (T) vs. susceptibility, all three intrusions are dominated by an oblate magnetic fabric. (C) Shape (T) vs degree of anisotropy (P_j). Also displaying an oblate magnetic fabric.

The mean degree of anisotropy (P_j), shape factor (T), susceptibility, along with the declination and inclination for Kmax and Kmin are listed in table 1. Figure 14 shows a direct comparison of the scalar parameters in each intrusion. Although the degree of anisotropy is roughly the same between the NLMD and SKI, the NLMD is less oblate,

and has higher mean susceptibility than the SKI and BEI. The large susceptibilities associated with the NLMD and the SKI suggests a higher concentration of ferromagnetic material in those intrusions that there is in the BEI.

The BEI also displays an oblate magnetic fabric, but in general has a much higher degree of anisotropy than the NLMD and SKI and a much lower range of susceptibilities. The NLMD and the SKI have larger amounts of magnetite that would result in a larger range of susceptibilities.

Figure 14 shows the degree of anisotropy versus the shape factor. On average, all the intrusions are oblate in shape, although there are a few samples which have a T<0, and therefore have a prolate magnetic fabric. The samples that exhibit both weak susceptibility and prolate fabrics may be the result of distribution anisotropy (Stephenson, 1994). Distribution anisotropy is the result of interacting multidomain magnetite grains that are separated by a distance smaller than their diameter. Stephensn, (1994) suggests

Mean AMS Scalar Parameters and Mean Directions

Intrusion	P_j	T	Mean k ($x10^{-6}$) (SI)	Kmax Dec (°)	Kmax Inc (°)	Kmin Dec (°)	Kmin Inc (°)
NLMD	1.07	0.88	18564.39	234.5	19.5	89.1	66.7
SKI	1.08	0.97	10200.86	14.5	22.5	145.2	57.5
BEI	1.25	0.72	7218.50	357.2	24.3	123.9	52.9

Table 1: Mean scalar parameters, susceptibility, Kmax, and Kmin for the NLMD, SKI, and the BEI.

that if the magnetite grains are distributed in a line, then they will produce a prolate fabric, and when they are distributed like a sheet, they will display an oblate fabric.

Analysis of AMS Fabrics

In general, magnetic fabrics can be described as having either a normal of an inverse magnetic fabric. When a rock has a normal fabric the magnetic fabric is generally oriented parallel to sub-parallel with the rocks foliation. In other words, K_{max} and K_{int} are contained in the mineral fabric. When K_{max} is perpendicular to a rock's mineral foliation, it has an inverse magnetic fabric. Only one site from the NLMD had samples that exhibited inverse fabric.

AMS samples from the northernmost section of the BEI were collected from both the inner ring of gabbro as well as the outer layer of troctolite. No samples were collected from the southern portions of the BEI because outcrop exposure is very sparse. Mineral foliations from this area show concentric strikes that dip inward, ranging from vertical along the northwestern margin to horizontal at Tonic Lake. There is also a large gravity high along the western margin of the northern BEI, which is thought to represent the original feeder to this system of intrusions (Peterson, personal conversations). The tilt-corrected AMS data from both the gabbro and the troctolite sections of the BEI dip towards the Tonic Lake region, consistant with the hypothesis that the mantle feeder originated beneath the northern portions of the BEI. The Bald Eagle troctolite samples have an uncorrected mean Kmax declination and inclination of 352.9º/5.0º, and a tilt-corrected mean Kmax declination and inclination of: 357.2º/24.3º(C and D in Figure 15). The Bald Eagle Gabbro (Tonic Lake samples) yields a mean Kmax declination and inclination of 307.5º/8.8º, and a tilt-corrected: 306.1º/33.6º(A and B in Figure 15).

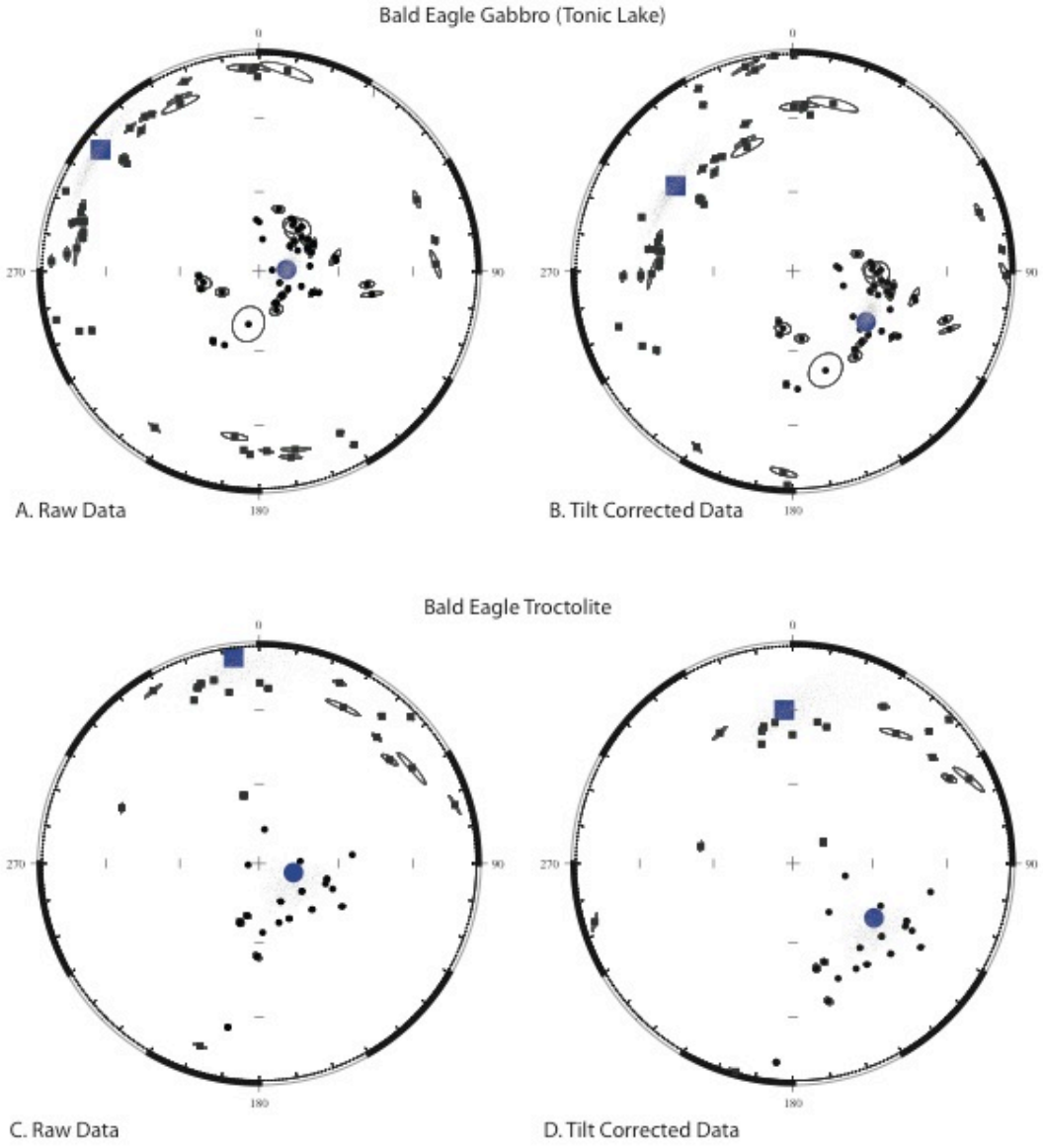

Figure 15: Southern hemisphere equal area steronets for the Bald Eagle gabbro (Tonic Lake), and the Bald Eagle troctolite. Squares and circles represent the Kmax and Kmin directions, respectively. The ellipses are the error associated with the data point. Larger blue squares and circles represent the mean Kmax and Kmin directions. Gray circles represent points produced using bootstrapping statistics. (A) is the uncorrected data for the Bald Eagle Gabbro with a Kmax and Kmin of 307.5°/8.8° and 100.0°/80.1°. (B) is the tilt corrected data for the Bald Eagle Gabbro with a Kmax and Kmin of 306.0°/33.6° and 124.7°/56.4°. (C) is the uncorrected data for the Bald Eagle troctolite with a Kmax and Kmin of 352.9°/5.0° and 104.9°/76.7°. (D) is the tilt corrected data for the Bald Eagle troctolite with a mean Kmax and Kmin of 357.2°/24.3° and 124.0°/49.9°.

The AMS results from the NLMD can be divided into two groups: the central portion of the dike and its mouth. The Kmax for the central region dips shallowly toward

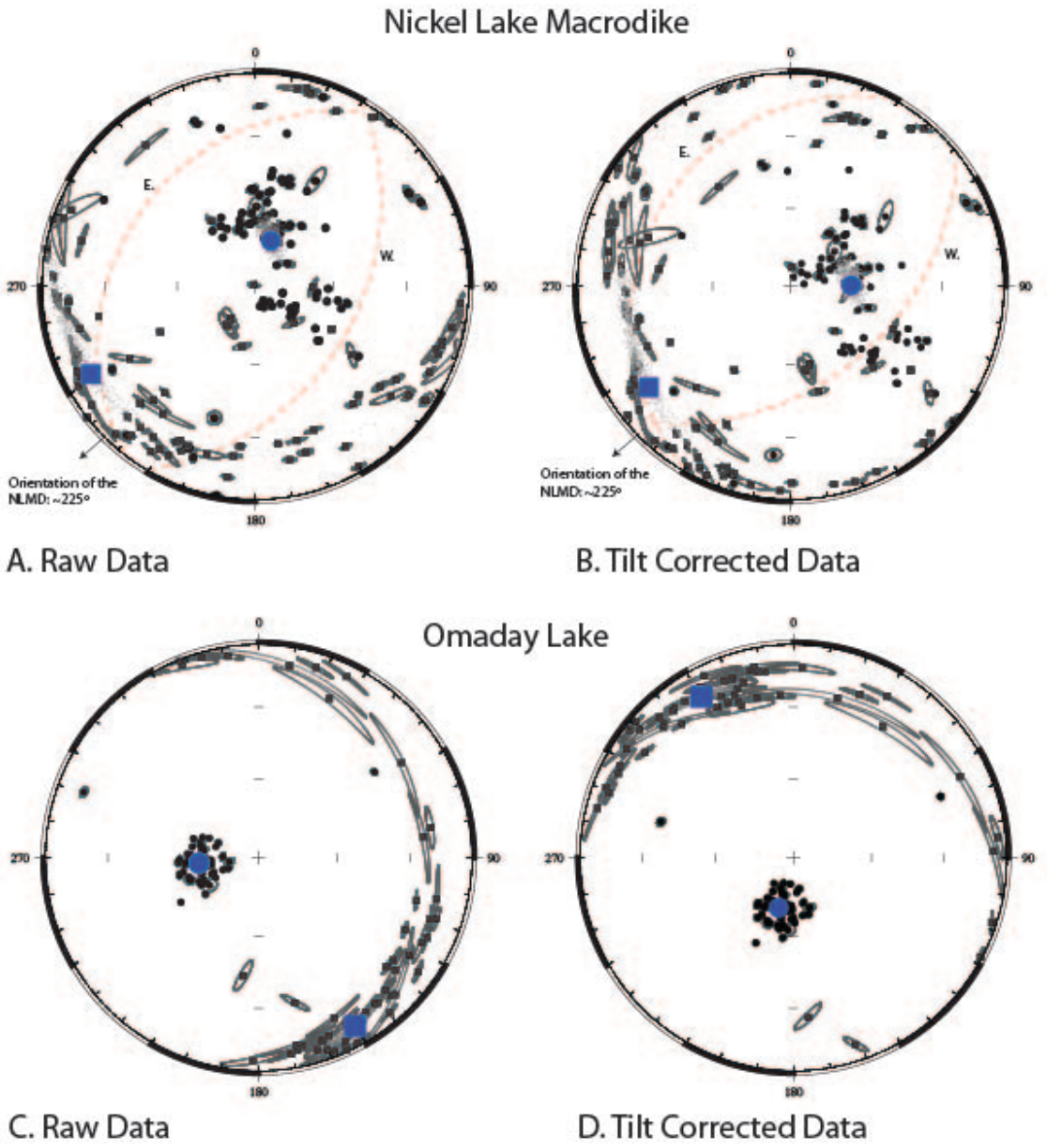

Figure 16: Southern Hemisphere equal area stereonets for the NLMD and Omaday Lake. Squares indicate Kmax, circles indicate Kmin, and the larger blue squares and circles represent the Kmax and Kmin directions. Gray clouds of data represent points generated using bootstrapping statistics. (A) is the raw data dor the NLMD with a mean Kmax and Kmin of 241.9°/13.7° and 18.9°/71.6. (B) is the tilt corrected data with a mean Kmax and Kmin of 234.5°/19.5° and 89.1°/66.7°. Both the raw and tilt corrected data suggest flow was subhorizontal, parallel to the strike of the NLMD. The red dashed lines in A and B represent the foliation planes of the Western (W), and Eastern (E) margins of the NLMD. (C) is the unrotated data for Omaday Lake samples near the mouth of the dike with a mean Kmax and Kmin of 146.8°/11.2° and 264.7°/67.0°. (D) Tilt corrected Omaday Lake samples with a mean Kmax and Kmin of: 146.9°/-13.3° and 196.3°/70.0°.

the northeast-southwest direction. The mean Kmax declination and inclination for the non tilt-corrected data is 241.9º/13.7º, and tilt-corrected values of 234.5º/19.5º (A and B

in Figure 16).

The mineral foliation of the NLMD was also analyzed to see how well it corresponded with the magnetic fabric. Instead of finding a single plain of foliation, the mineral foliations group into two geographically dependent clusters. The mean direction was then calculated for each cluster of data. The corresponding planes of foliation for these two clusters of data have been interpreted as the imbricated foliation of the eastern and western margins of the dike. The mean Kmax declination and inclination has been interpreted as the overall direction of magma flow, which is parallel to the axis of the dike, and falls between the mineral foliation plains.

The samples collected from the mouth of the dike, near Omaday Lake, also have a shallowly dipping magnetic fabric; only this time, in the northwest-southeast direction with a non-tilt-corrected mean Kmax declination and inclination of 146.8º/11.2º, tilt corrected: 146.9º/-13.2º (C and D, figure 16). This change in flow direction may be due to a large anorthositic block near the mouth of the dike. This would have blocked the entrance to the SKI, causing the flow to change its course by squeezing between the anorthositic inclusion and the anorthositic wall rock, causing flow to curl off toward the southeast (See figure 18a).

The SKI AMS data is much more turbulent and multidirectional than the NLMD, as would be expected from a transition from constrained flow within the NLMD into a more open, low-energy regime. Each site sampled within the SKI gives a slightly different flow vector depending on the geographic location of the sample. For example, samples from the western margin of the SKI had AMS vectors that suggest flow towards

the west. Despite the multidirectional nature of the SKI, both a mean and a normalized mean were calculated. The mean Kmax declination and inclination: 8.6º/8.6º, tilt-corrected to: 14.6º/22.5º.

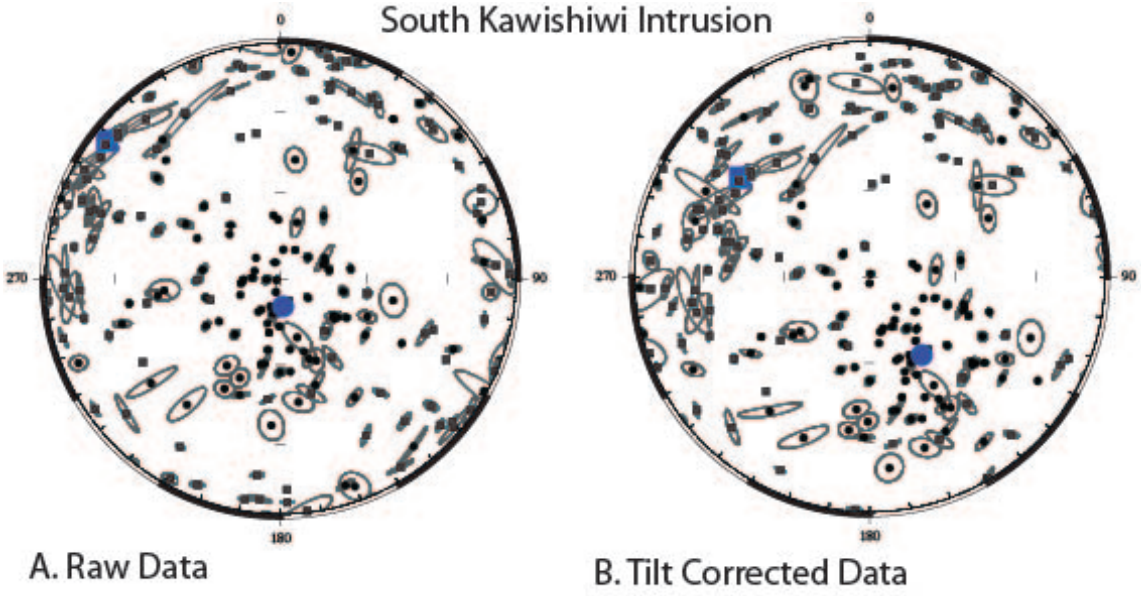

Figure 17: Southern hemisphere equal area projection plot for the SKI. Squares indicate the Kmax directions, and circles indicate the Kmin directions. Ellipses represent the error on each measurment. Blue cirlces and squares represent the normalized mean Kmin and Kmax, respectively. For the raw data the normalized Kmax and Kmin are 302.9º/4.9 and 173.3º/81.1º, and the tilt corrected normalized mean Kmax and min are 301.2º/29.3º and 146.2/58.2º, respectively. These plots highlight the multidirectional nature of the flow within the SKI. The weighted mean suggests some flow preference toward the NW (toward the basal contact and the Nokomis Deposit).

The normalized mean Kmax declination and inclination: 302.9º/8.6º (Figure 15, A and B), tilt corrected to: 301.2º/29.3º. (Figure 17, C and D). The discrepancy between the weighted and unweighted mean is a due to the turbulent, multidirectional flow within the SKI.

The AMS data thus far supports the hypothesis proposed by Peterson, (2008). Unidirectional flow within the NLMD was subhorizontal, parallel to the strike of the dike. Upon exiting the NLMD, flow became much more turbulent and multidirectional as the SKI magma chamber was filled. There may be some evidence for a vertical feeder

dike in the Tonic Lake region of the BEI, but a more intensive study in that area should be completed for a better understanding of the plumbing system associated with these intrusions (see Figure 18b).

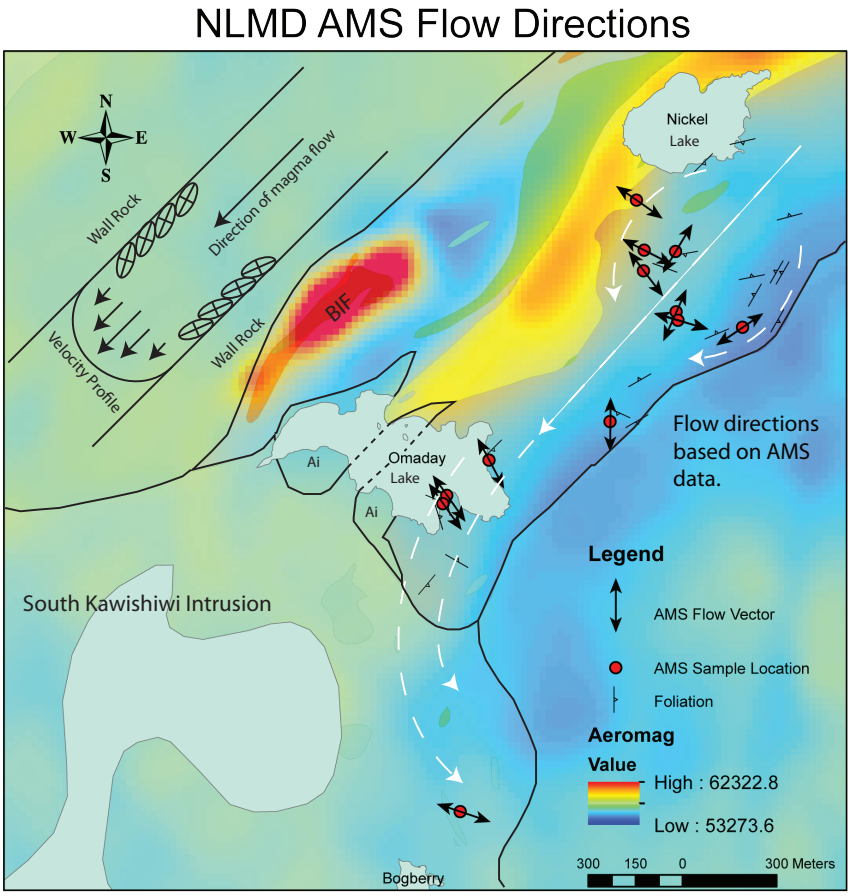

Figure 18a: The aeromagnetic data has been projected ontop of the NLMD geology. To highlight the magnetic anomalies as well as to show the proposed magma flow through the dike based on the AMS results. Magma traveled subhorizontally along the strike of the macrodike, there is a zone of turbulence as the dike bottlenecks approximatly half way between Nickel Lake and Omaday Lake, the flow then must squeeze in between the anorthositic inclusion(Ai) and the anorthostic wallrock, causing flow to veer off toward the SW upon exiting the NLMD. The magnetic high on the western margin of the dike is due to an outcrop of the Banded Iron Formation (BIF). The majority of the samples were collected on the eastern most layer, the Nickel Lake Oxide Gabbro (N-xG), in a magnetic low. Schematic of the fluid velocity profile through a dike. Note the maximum velocity is at the center of the dike, and there is zero velocity along dike margins. This creates the conditions neccessary for shearing to cause particle imbrication as illustrated by the ellipses.

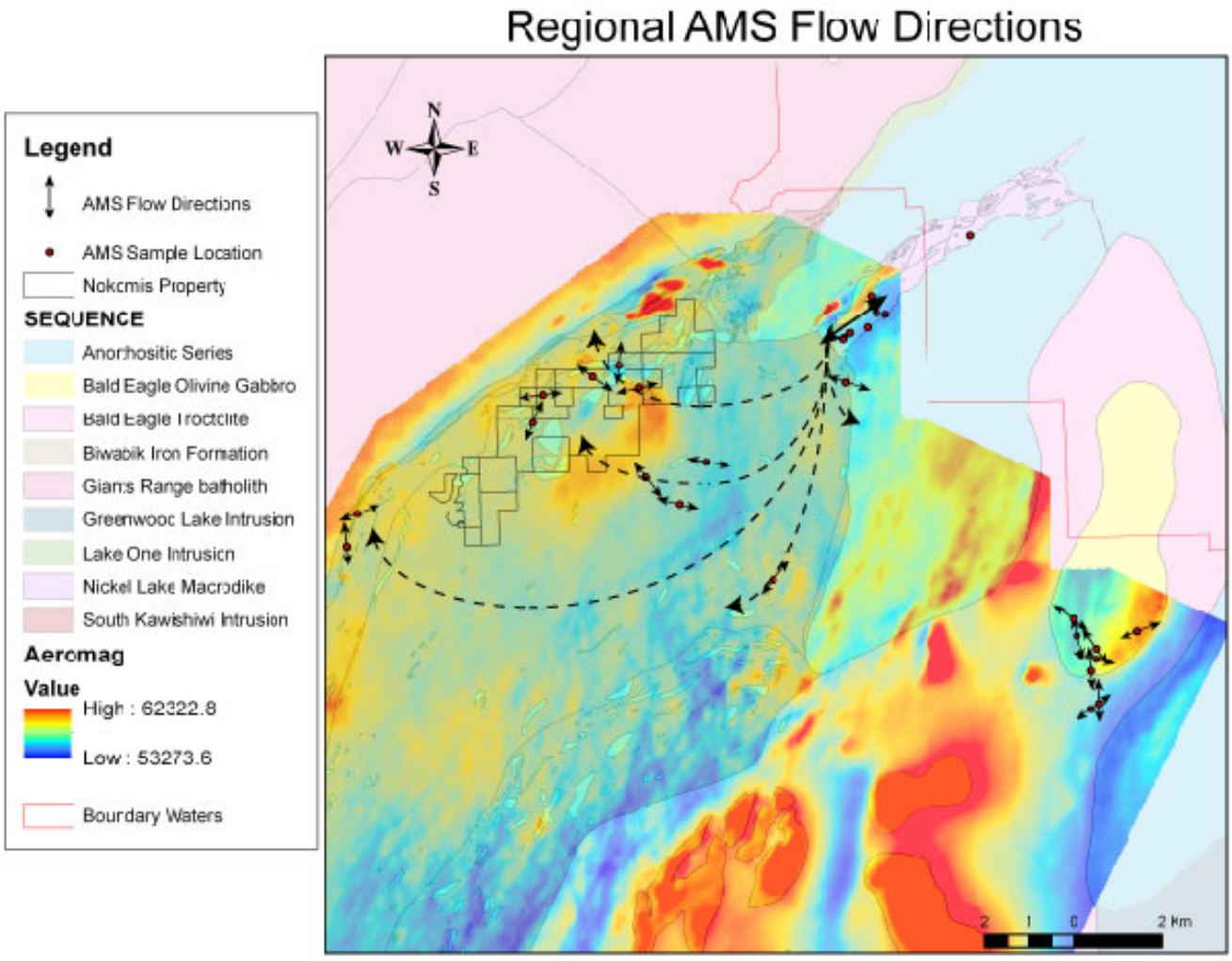

Figure 18b: Regional flow from the NLMD into the SKI intrusion as determined by AMS. As the magma exited the NLMD, it became multidirectional, while trending toward Giants Range Batholith (GRB) footwall rocks. The wall rock (blue) is the Anorthositc Seriers (An).

Paleomagnetic Directions

Characteristic remanent magnetizations (ChRMs) were calculated for 65 samples 21 from the NLMD, 22 from the SKI, and 22 from the BEI intrusions. The Mean

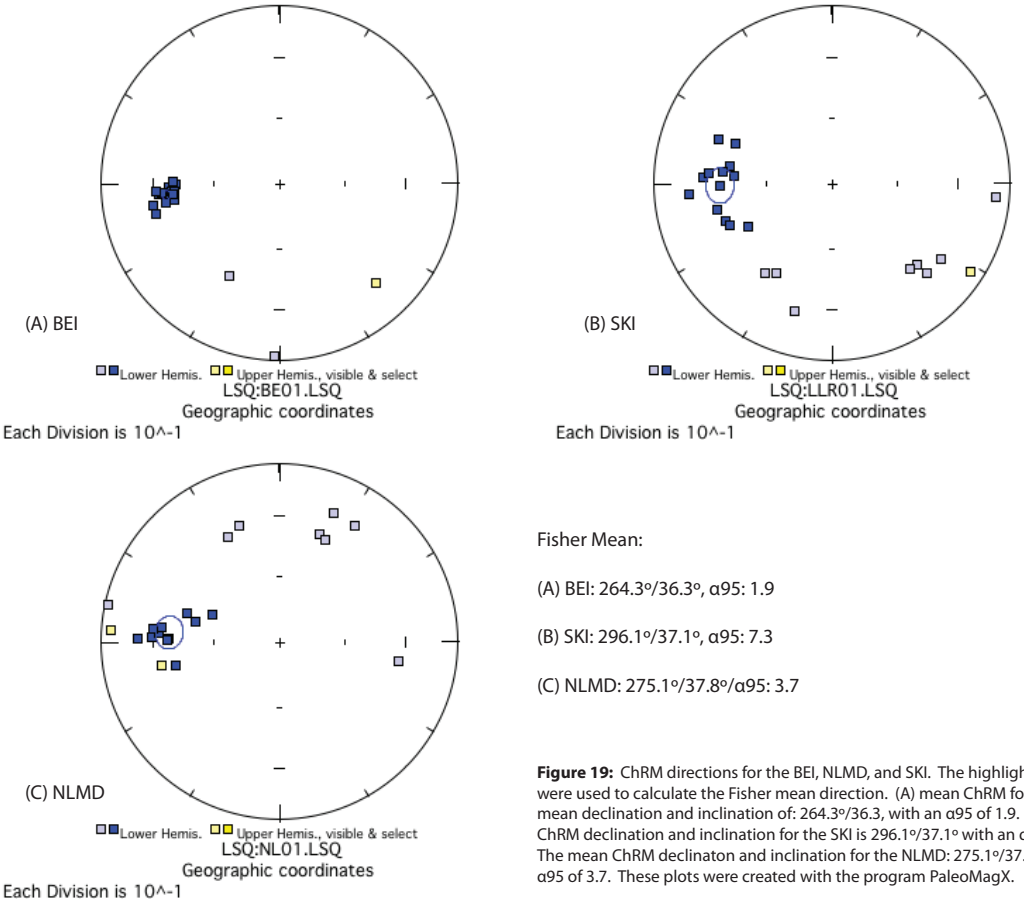

Figure 19: ChRM directions for the BEI, NLMD, and SKI. The highlighted squares were used to calculate the Fisher mean direction. (A) mean ChRM for the BEI has a mean declination and inclination of: 264.3º/36.3, with an α95 of 1.9. (B) The mean ChRM declination and inclination for the SKI is 296.1º/37.1º with an α95 of 7.3. (C) The mean ChRM declinaton and inclination for the NLMD: 275.1º/37.8º, with an α95 of 3.7. These plots were created with the program PaleoMagX.

direction was calculated using least-squares principle component analysis (Kirschvink, 1980) (Figure 19). The AFD results are shown in Table 2. The NLMD produced a mean un-rotated direction of 275.1º/37.8° with a α_{95} of 3.7°, 269.1º/37.1º with a α_{95} of 7.3° for the SKI, 264.3º/36.3º with a α_{95} of 1.9° for the BEI.

The agreement between the paleomagnetic data from each intrusion is consistent with the hypothesis that the intrusions all formed at roughly the same time, perhaps from the same feeder system. Variations in the declination range 10.8º between the NLMD and

the BEI, but this difference is rendered negligible when margins of error are taken into account.

The thermal demagnetization results were largely inconclusive. After the 450º

Chandler, (2009)					
Rock Type	Susceptibility (SI)	NRM (A/m)	Q	NRM Dec/Inc (°)	ChRM Dec/Inc (°)
BE G.	0.004	3.78	21	291/30	-
BE T.	0.009	1.2	2.8	303/55	-
Basal T.(SKI)	0.016	3.2	4.2	284/44	-
NLMD	-	-	-	-	-
Finnes, (2012)					
Rock Type	Sucseptibility (SI)	NRM (A/m)	Q	NRM Dec/Inc (°)	ChRM Dec/Inc (°)
BE G.	0.004	4.18	25.9	205/33	264/36
BE T.	0.008	2.25	17.3	261/16	
SKI	0.013	6.68	11.6	282/20	269/37
NLMD	0.027	2.27	2.7	340/40	275/38

Table 2: This table compares the susceptibility, ChRM, and the direction and intensity of the NRM between this study and the study by Chandler, 1990.

heating step the NRM directions became randomized, resulting in unreliable ChRM directions. The oxidation of pyrite to hematite occurs between 450º and 550º (Bollin, 1970). Evidence for pyrite was observed in the temperature versus magnetization curves, as well as the high temperature susceptibility curves. Because the experiment was conducted in air, it is possible that the transformation from pyrite to hematite disrupted the demagnetization sequence. This issue was probably compounded by the fact that samples were packed too closely together in the furnace during demagnetization steps. (To save time about 30 samples were tightly packed and thermally treated together.) This may have allowed the magnetic fields of the individual samples to interact with each

other upon cooling, thus changing the remanence of individual specimens. It is worth noting for future paleomagnetic measurements, that the samples should be given ample space during thermal treatment.

Chandler (2009) reported NRM measurements for the BEI, and the Basal Troctolite (including the SKI). However, the mean NRMs calculated in this study do not agree well with the values produced by Chandler (See Table 2). While the source of this discrepancy remains unclear, the values reported by Chandler (1990) are NRM values, not ChRMs, and it may be that greater agreement may have been reached if these earlier samples were subjected to alternating field or thermal demagnetization.

Q-Values

Q-Values can be used to characterize local magnetic anomalies. In the northern hemisphere, Q < 1 indicates that the sample's magnetic signature is dominated by induced magnetization, and the aeromagnetic anomaly associated with the sample should be positive and parallel to the current geomagnetic field.

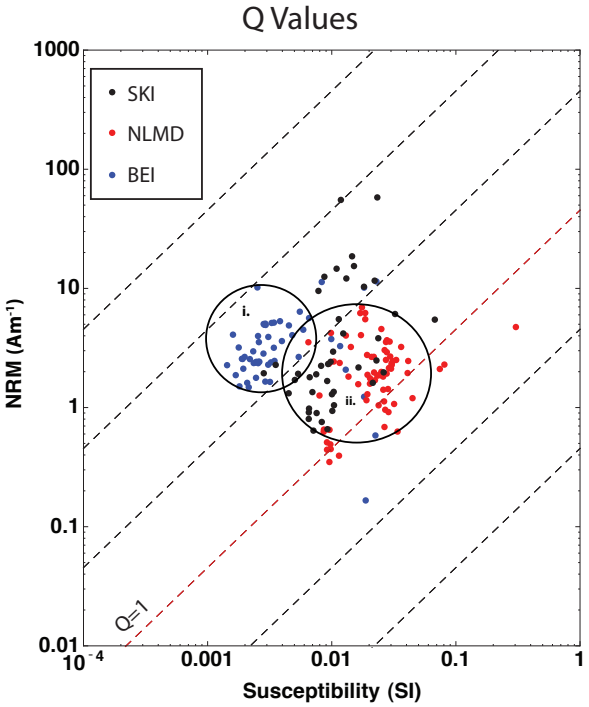

Figure 20: Q values fr the NLMD, SKI and Bald Eagle Intrusions. Red Dashed line indicates where Q=1. i. Is the cluster of data represeting the BEI with a mean Q>10 indicating that the magnetic anomalies associated with these samples have a strong dependance of the Natural Remanent Mangetization. ii. is the cluster of data associated with the NLMD and the SKI, with a mean Q>1 indicating that the magnetic anomalies associated with these samples have a magnetic signiture that is dominated by the NRM.

Q values greater than 1 indicate that the rock's aeromagnetic anomaly will be dominated by the remanent magnetization. If J_r is parallel to the modern field and has a relatively high magnitude, one would expect a large positive anomaly. In contrast, if J_r is anti-parallel to the modern field and has a relatively high magnitude, then the expected anomaly should be large and negative.

As part of an airborne geophysical survey, Geotech was contracted by Duluth Metals Inc. to collect aeromagnetic data during the summer of 2010, using 100 meter line spacing at an elevation of 100 m. In the Reduced To Pole (RTP) magnetic data, there is evidence for both positive and negative magnetic anomalies in the NLMD, SKI, and the BEI. In general, a positive magnetic anomaly suggests that the magnetic signature is associated with the modern inducing field. Q-values for rocks from the Nokomis Deposit are shown in Figure 20. Of the 186 samples measured, 96% had Q values greater than 1, suggesting that even the positive magnetic anomalies may be associated with contributions from the rocks' remanent magnetization. Chandler, 1990 interpreted some of the magnetic highs in the BEI to be associated with large (~10 m scale) inclusions basaltic hornfels. However, field mapping and the Duluth Metals drilling program in the BEI suggest that the magnetic highs are actually associated with deep-seated anorthositic inclusions. These anorthositic inclusions often contained high concentrations of course-grained iron oxide minerals, which are likely to have high susceptibilities, low coericivities, and contribute to Q values less than 1. Thus, it is possible that the samples measured at the surface contribute very little to the observed positive magnetic

anomalies, and that the anomalies are due to the induced magnetization associated with anorthositic inclusions entombed within the BEI.

Figures 17 and 18 show the aeromagnetic data of the study area, overlain on top of the geologic map by Peterson, (2001). This allows for the direct comparison between the anomalies and the geologic bodies. An obvious relationship exists between the large positive aeromagnetic anomalies and the boundaries of the BEI. The outer band of troctolite in the northern section of the intrusion is a distinctive negative anomaly, while the inner band of gabbro has a strong positive anomaly. As mentioned above, most of the BEI samples have Q>1, and 89% have Q>10, indicating the dominance of the remanent magnetization over induced magnetization (Figure 20).

In the NLMD 89% of the samples have a Q>1, again indicating a dominance of the remanent magnetization over the induced magnetization. The average NRM in the NLMD is of the same order of magnitude as the BEI, but the average susceptibility is an order of magnitude larger resulting in a smaller Q value.

It is likely that many of the positive magnetic anomalies in the SKI and the NLMD are also due to large xenolithic inclusions. Indeed, the largest positive anomaly on the western margin of the NLMD has been identified during geologic mapping as a large xenolith of Banded Iron Formation.

100% of the Q values measured from troctolitic rocks within the SKI are greater than 1, and 15% > 10. This is again consistent with a model where the NLMD and the SKI are genetically related. If this model is true, and there was a hiatus between the emplacement of the NLMD/SKI and the subsequent magmatic pulse that emplaced the

BEI, then it is not surprising that the NLMD and SKI Q values cluster together, separate from the Q values associated with the BEI.

Thin Section Analysis

To further characterize the magnetic mineralogy present in the Nokomis Deposit, thin sections were created from representative samples from the NLMD and SKI. Thin sections were analyzed using both plane-polarized light (PPL), and cross polarized light (CPL) on a standard petrographic microscope.

In the NLMD oxide gabbro, FeTi-oxides (Figures 21) occur as 0.5 to 1 mm long, needle-shaped inclusions exsolved within ophitic pyroxene. The paragenesis of these inclusions was examined by Feinberg et al., (2004), who showed that the exsolved inclusions frequently display SD and PSD magnetic properties and are elongated along two crystallographic directions (Figure 22) within the host pyroxene, the *a*- and *c*-axes. These two elongation directions produce a strongly oblate AMS fabric within a single pyroxene crystal. If the bulk rock contains a strong silicate fabric, then the bulk rock will exhibit a similarly oblate magnetic fabric. Plagioclase grains exhibited strong polycrystalline albite twinning. Perhaps the most exciting discovery in this rock unit was a ~6 mm ductily deformed, bent plagioclase lath (Figure 23). Bourdreu and McBirney (1997) suggest that this is a rare find, and may suggest that gravitational settling aided in the formation of the mineral foliation.

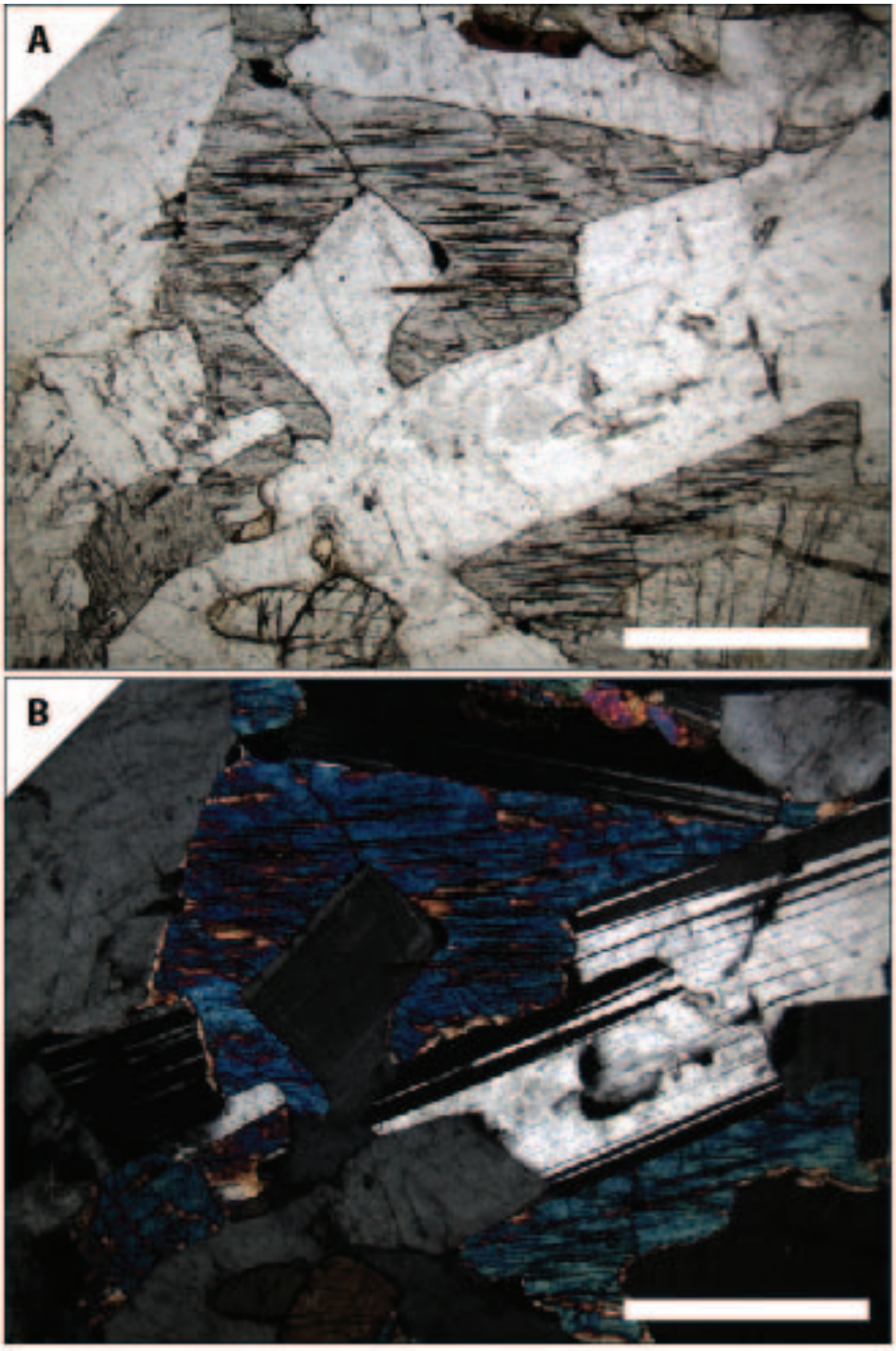

Figure 21: A. Plane polarized light image of elongated FeTi-oxide inclusions exsolved in clinopyroxene within the oxide gabbro of the Nickel Lake Intrusion (N-xG). The same horizontally oriented inclusions can be observed above and below the plagioclase grain in the center of the image, which is evidence of the pyroxene's ophitic texture. B. Cross-polarized light image of A, with the pyroxene showing the same birefringence color on either side of the plagioclase. Scale bar is 1 mm.

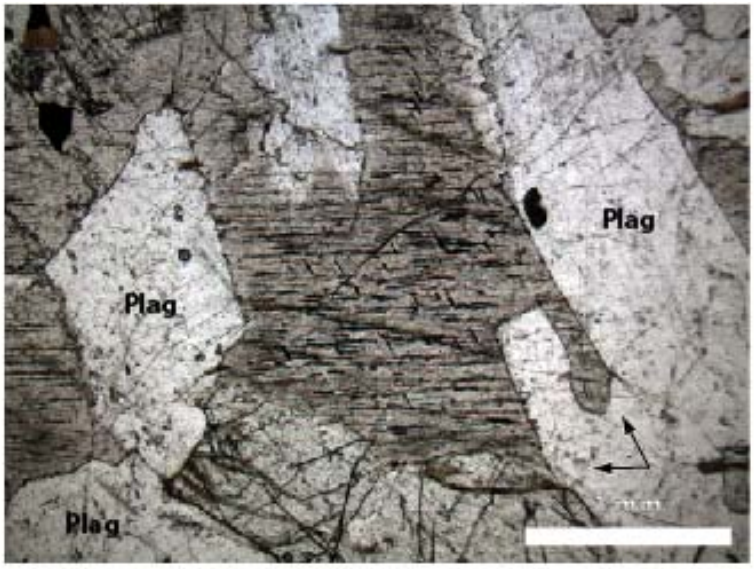

Figure 22: Plane polarized light image of elongated, needle-shaped FeTi-oxide inclusions exsolved in clinopyroxene within the augite-bearing troctolite of the South Kawishiwi Intrusion (S-pT2). There are two orientations of inclusions indicated by the arrows by the scale bar: one subparallel to the clinopyroxene [100] and another subparallel to the clinopyroxene [001].

Figure 23: Cross-polarized light image of the oxide gabbro of the Nickel Lake Intrusion (N-xG) showing ductile deformation of plagioclase lath and sub-ophitic texure of pyroxene.

The Nickel Lake Layered Troctolite samples had a much higher modal abundance of olivine (~30% to 35%) than did the N-xG samples. The same needle-shaped inclusions of FeTi-oxides were observed in the ophitic pyroxene crystals, but courser interstitial FeTi-oxide grains were also observed between the olivine and plagioclase

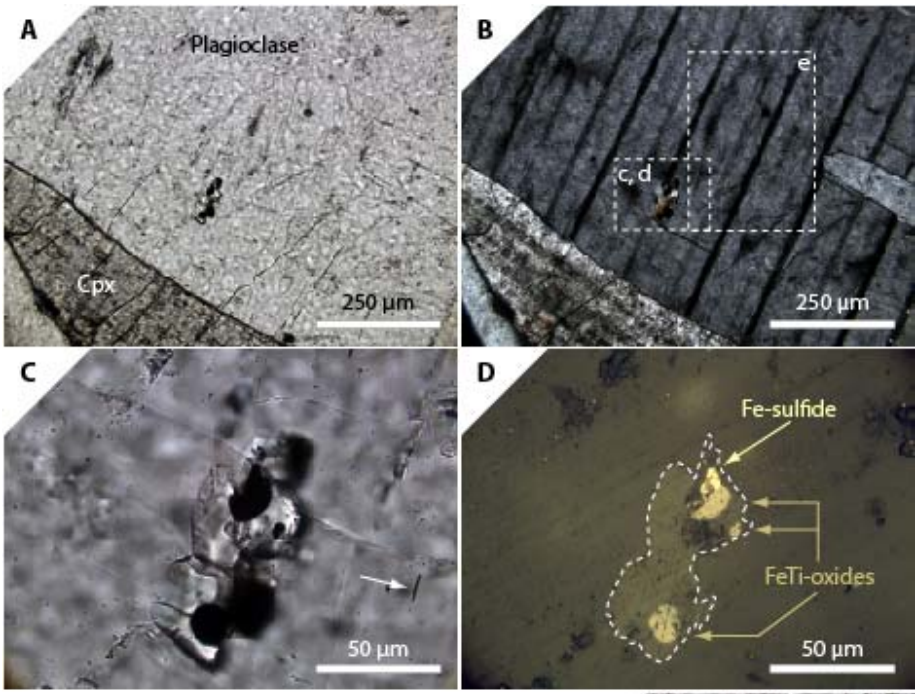

Figure 24: Fe-oxide and Fe-sulfide inclusions in plagioclase. in the augite troctolite of the South Kawishiwi Intrusion. A) Plane polarized light (PPL) image of clinopyroxene (Cpx) and plagioclase. Plagioclase contains exsolved, needle-shaped FeTi inclusions faintly visible in the center and upper portions of the image (see Fig. XE) and occluded Fe-sulfide minerals. B. Cross-polarized light image of A showing polysynthetic albite twin boundaries in plagioclase. Dashed box shows the extents of C, D, and E. C. PPL image of an occluded melt inclusion in plagioclase. White arrow points to an example of a needle-shaped, exsolved FeTi-oxide inclusion. D. Reflected light image of C showing the presence of both Fe-sulfide and FeTi-oxide grains. Dashed line shows the extent of the melt inclusion. E. PPL image of exsolved, needle-shaped inclusions trending NNE-SSW in plagioclase.

grain boundaries.

In the SKI, the same needle-like FeTi-oxide inclusions (Figure 24) were observed in both the anorthositic troctolite and the augite-bearing troctolite. In addition, euhedrally shaped titanomagnetite grains were found occluded within large plagioclase crystals. In some instances, symplectites (Figure 25) formed between the contacts of the FeTi-oxides and the host plagioclase crystals. Symplectites are a disequilibrium texture that are often associated with slowly cooled intrusions.

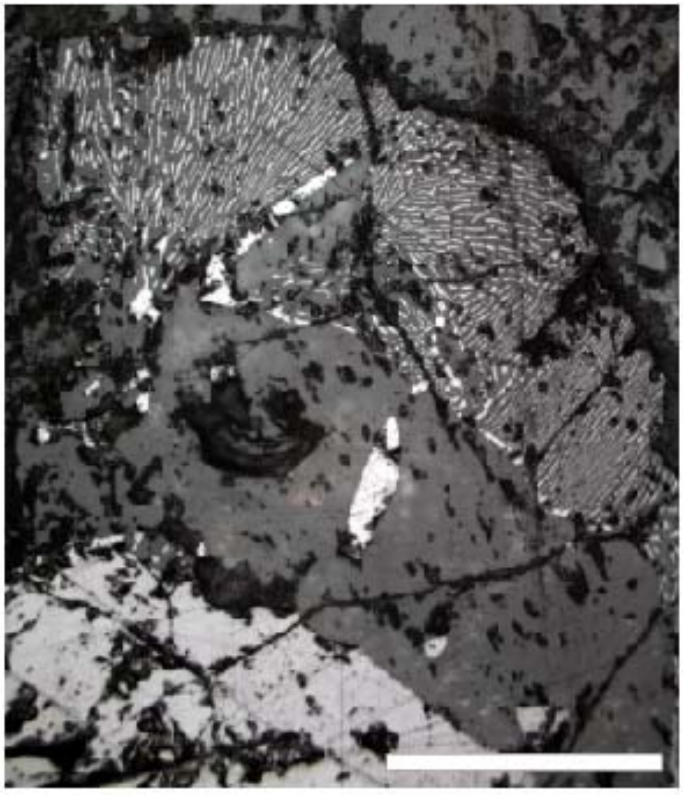

Figure 25: Reflected light image of symplectite in the augite troctolite of the South Kawishiwi Intrusion. The light colored material in the symplectite is titanomagnetite, as are the medium grain in the center of the image and the large grain at the bottom. The gray material is feldspar. Scale bar is 250 µm.

VI. Discussion

Age relationships between the different plutons.

Hoagland (2010) used U-Pb techniques to report an age of 1095.64±0.19 Ma for the BEI. Unfortunately, no age was reported for the NLMD or the SKI. Thus, it is not yet possible to use radiometric techniques to constrain the emplacement order of the individual intrusions of the Layered Series.

Miller and Severson, (2002) developed an emplacement model for the Layered Series intrusions based on the cross cutting relationships indicated by the aeromagnetic study of study Chandler, (1990). They proposed a successive overplating from northwest to southeast creating the following emplacement history (from oldest to youngest): Partridge River Intrusion (PRI), South Kawishiwi Intrusion (SKI), Wilder Lake Intrusion (WLI), Lake One Troctolite (L1), Tuscarora Intrusion (TI), Boulder Lake Intrusion (BLI), Greenwood Lake Intrusion (GLI), Bald Eagle Intrusion (BEI), and the Duluth Layered series (DLS).

Flow Dynamics during pluton emplacement

Compositional layering and foliation in mafic intrusions can form due to a number of different processes (Nashlund and McBirney, 1996), but in the NLMD, SKI, and BEI the layering and foliation appear mainly to be the result of magmatic flow processes and gravitational settling. Other than small amounts of localized hydrothermal alteration, there is no evidence of brittle deformation on the macro or micrometer scale.

Gravitational settling usually occurs in a static magma chamber that has little to no flow associated with it, and can create relatively weak oblate fabrics where lineation is virtually absent (Nicolas, 1992). The bent plagioclase lath observed in thin section offers hard evidence that late stage compaction influenced the mineral fabric in the NLMD. However, the magnetic fabric in these rocks is strong, not weak, and the influence of magmatic flow processes seems to be the dominant control on mineral fabric.

According to Den Tex (1969) and Knight and Walker (1988) mineral foliation is a common byproduct in dense flowing fluids, where particles are able to physically interact. These foliations often form at some angle to the general flow plain. This produces a kind of imbrication, where the foliation points in the general direction of magma flow. The strong imbrication observed in the AMS data in the NLMD suggests that magmatic flow was primary mechanism responsible for fabric development.

Economic implications for mineral exploration

One of the high costs associated with exploration is due to a technique known as step-out drilling, where a grid pattern of drill holes is used in hopes of intersecting a economically important mineral deposit. This practice virtually ignores any potential contribution that a deeper understanding of the regional geology may provide to an exploration program. Techniques such as AMS offer exploration companies the opportunity to more efficiently focus their drilling efforts.

The anisotropy of magnetic susceptibility is a powerful tool seldom used by exploration companies. If properly integrated within an exploration program, an AMS

study has the potential to reduce exploration costs. AMS provides information about magmatic flow directions and magma system dynamics that can focus the location of exploration drill holes. Other information such as the degree of anisotropy, and the shape parameter, have the potential to provide a better understanding of rate of magmatic flow and shear stresses. Understanding the origin of a mineral fabric is important when studying the initial conditions of an igneous intrusion that might host potential ore body.

AMS is not the only rock magnetic tool available to exploration companies. Magnetic mineralogy can be determined using simple Curie temperature experiments. Although not possible in this study, paleomagnetic studies can provide relative, and perhaps even absolute, ages for mineral deposits by comparing the virtual geomagnetic pole of a site to a reference Apparent Polar Wander Paths (APWP). Q-values can help exploration companies better interpret local magnetic anomalies and be used as an intrinsic qualifier when mapping and identifying potentially new and interesting igneous intrusions.

Further Work

To completely verify the model proposed by Peterson, (2008) it may be necessary to collect more samples for AMS from the SKI, NLMD, and BEI. A detailed AMS study of the individual flows within the NLMD could be used to confirm the complete emplacement history of the NLMD. Samples should also be collected from the northernmost portion of the NLMD to confirm that flow originated from beneath the BEI.

AMS investigations do not have to be limited to the exploration phase, but could be used equally well in the mine development phase. Once an intrusion has been identified, it may be useful to know how the magma was traveling inside the deposit. This can be accomplished by measuring the AMS in oriented core collected individual boreholes. Even though not all drill cores are oriented, it is possible to get AMS results from unoriented drill core using a technique called Paleomagnetic Reorientation of unoriented drill core.

Because the up and down direction on drill core is known, the mean ChRM obtained from nearby outcrops can be used as a proxy to reorient unoriented drill core. The idea is simple enough:

Step 1: create an arbitrary azimuth reference line on the drill core sample.

Step 2: measure the CHRM of the drill core.

Step 3: determine the angular difference between the outcrop CHRM and the drill core CHRM.

Step 4: rotate the arbitrary reference line by the amount computed in step 3. Step 5: mark sample with a new rotated reference azimuth and use this to measure the AMS.

Understanding how magma traveled at depth would help determine where the next borehole should be drilled, and eliminate drilling any unnecessary boreholes. By gaining a deeper understanding of where the magma traveled and where it came from, AMS can help exploration geologists save money, locate ore, and better understand the initial conditions.

VII. Conclusions

AMS data from the NLMD confirms the prediction that there was subhorizontal, unidirectional magma flow within the NLMD parallel to the strike of the dike. This data also confirms that there was complex, non-unidirectional flow within the SKI, with an average flow direction toward the basal contact where the Ni-Ci-PGE enrichment within the Nokomis Deposit is located. The AMS eigenvalues show that, in general, the magnetic fabric is oblate with a high degree of anisotropy. The magnetic fabric is imbricated along the dike margins, suggesting that magmatic shear stresses controlled the formation of both the mineral and magnetic fabric. The observation of a bent plagioclase lath suggests that late stage gravitational settling also may have modified the mineral and magnetic fabric.

The ChRM values show that the intrusions formed at roughly the same time, and there is some evidence for a temporal hiatus between the emplacement of the NLMD and the BEI.

Magnetic mineralogy and grain size analysis suggests that the primary magnetic carriers are PSD FeTi-oxides. Thin section observations confirm that the SPO of these grains is controlled by the SPO of the mineral foliation. The relatively high coercivity of the PSD grains creates conditions for a relatively stable remanent magnetization. This becomes especially apparent in the high Q-values, which suggest that the local magnetic anomalies are controlled primarily by the remanent magnetization of the rocks, rather than from a modern induced magnetization. In general, the NRM was observed to be most stable in the BEI, while the NLMD and SKI have less stable NRM's due to the

higher concentration of coarse-grained ferromagnetic minerals, such as titanomagnetite and pyrrhotite.

By confirming the model proposed by Peterson, (2001), this study demonstrated that rock and paleomagnetic techniques can be used in the exploration industry to characterize an igneous body of economic interest. In particular the anisotropy of magnetic susceptibility proved to be a powerful tool for determining flow directions, and we encourage others to implement such studies before beginning any serious drilling campaign.

VIII. Bibliography

Aziz-ur-Rahman, Gough, P.I. and Evans, M.E., 1975. Anisotropy of magnetic susceptibility of the Martin Formation, Saskatchewan, and its sedimentological implications. Candian Jouranal of Earth Sciences.

Borradaile, G.J., Jackson, M., 2004. Anisotropy of magnetic susceptibility(AMS); magnetic petrofabrics of deformed rocks. In: Mart´ın-Hern´andez, F., L¨uneburg, C. M., Aubourg, C., Jackson, M.(Eds.), Magnetic Fabric: Methods and Applications. Geol. Soc. Spec. Publ. 238, pp. 299–360.

Boudreau, A.E., McBirney, A.R., 1997. The Skaergaard layered series. Part III. Non-dynamic layering. J. Petrol. 38, 1003–1020.

Chandler, V.W., 1990. Geologic interpretation of gravity and magnetic data over the central part of the Duluth Complex, northeastern Minnesota. Economic geology and Bulletin of the Society of Economic Geologists, p. 816-829.

Davis, D.W., and Paces, J.B., 1990. Time resolution of geologic events on the Keweenaw Peninsula and implications for development of the Midcontinent Rift system.
Earth and Planetary Science Letters, v. 97, pp. 54-64.

Davis, D.W., and Green, J.C., 1997. Geochronology of the North American Midontinent rift in western Lake Superior and implications for its geodynamic evolution.
Canadian Journal of Earth Sciences, v. 34, pp. 476-488.

Day, R., Fuller, M., Schmidt, V.A., 1977. Hysteresis properties of titanomagnetites: grain-size and compositional dependence. Phys. Earth Planet. Int. 13, 260–267.

Dekkers, M.J., 1988 Magnetic properties of natural pyrrhotite Part I: Behavior of initial susceptibility and saturation-magnetization-related rock-magnetic parameters in a grain-size depedent framework. Physics of the Earth and Planetary Ineriors, 52, pg. 367-393.

Den Tex, E., 1969. Origin of ultramafic rocks, their tectonic setting and history; a contribution to the discussion of the paper 'The origin of ultramafic and ultrabasic rocks' by P.J. Wyllie. Tectonophysics 7, pg. 457–488.

Dulop, D.J., 2002. Theory and application of the Day plot (M_{rs}/M_s versus H_{cr}/H_c) 2. Application to data for rocks, sediments, and soils. Jouranal of Geophysical Research, Vol. 107. pg. 5-1 to 5-15.

Ernst, R.E., Baragar,W.R.A., 1992. Evidence from magnetic fabric for the flow pattern of magma in the Mackenzie giant radiating dyke swarm. Nature 356, pg. 511–513.

Ferré, E.C., Bordarier, C., Marsh, J.S., 2002. Magma flow inferred from AMS fabrics in a layered mafic sill, Insizwa, South Africa. Tectonophysics 354, pg. 1–23.

Ferré, E.C., 2002. Theoretical models of intermediate and inverseAMS fabrics. Geophys. Research Letters 29(7), 1127.

Feinberg, J.M., Scott, G.R., Renne, P.R., and Wenk, H.-R., 2004, Exsolved Magnetite Inclusions in Silicates: Features Determining Their Remanence Behavior: Geology, 33 (6), p. 513-516.

Fleet, M.E., Bilcox, G.A., and Barnett, R.L.,1980 Oriented magnetite inclusions in pyroxenes from the Grenville province. Canadian Mineralogist, 18, pg. 89-99.

Green, J.C., Phinney, W.C., and Weiblen, P.W., 1966, Geologic map of Gabbro Lake quadrangle, Lake County, Minnesota: Minnesota Geological Survey Miscellaneous Map Series M-2, scale 1: 31,680.

Grommé, S., Wright, T.L., Peck, D.L., 1969. Magnetic properties and oxidation of iron-titanium oxide minerals in Alae and Makaopuhi lava lakes, Hawaii. J. Geophys. Res. 74, 5277–5294.

Hargraves, R.B., Johnson, D., Chan, C.Y., 1991. Distribution anisotropy; the cause of AMS in igneous rocks? Geophys. Res. Lett. 18, pg. 2193–2196.

Hext, G., 1963, The estimation of second-order tensors, with related tests and designs, Biometrika, 50, P. 353-357.

Hoagland, S.A., 2010, U-Pb geochronology of the Duluth Complex and related hypabyssal intrusions: investigating the emplacement history of a large multiphase intrusive complex related to the 1.1 Ga Midcontinent Rift. M.S. thesis: University of Minnesota, Duluth, p.103.

Hrouda, F., 1982. Magnetic anisotropy of rocks and its application in geology and geophysics. Geophysical Surveyes 5:37-82.

Jeffery, G.B., 1922. The motion of ellipsoidal particles immersed in aviscous fluid. R. Soc. Lond. Proc., Ser. A 102, 169–179.

Jel´ınek, V., 1978. Statistical processing of anisotropy of magnetic susceptibility measured on groups of specimen. Studia Geophyzika et Geodetika 22, 50–62.

Jel´ınek, V., 1981. Characterization of the magnetic fabric of rocks. Tectonophysics, 79, T63–T67.

Kirschvink, J.L., 1980. The least-squares line and plane and the analysis of paleomagnetic data. Geophysical Journal of the Royal Astronomical Society, v.62, p.699-718.

Klewin, K.W., and Shirey, S.B., **1992.** The igneous petrology and magmatic evolution of the Midcontinent rift system. *Tectonophysics, v. 213,* pp. 33-40.

Knight, M.D., Walker, G.P.L., 1988. Magma flow directions in dikes of the Koolau Complex, Oahu, determined from magnetic fabric studies. Journal of Geophysical Research, Vol. 93, pg. 4301–4319.

Konigsberger, J. G., 1938. Natural Residual Magnetism of Eruptive Rocks Part II. Terrestrial Magnetism and Atmospheric Electricity, 43: pg. 299-320.

Maes, S.M., Tikoff B., Ferré, E.C., Browna, P.E., Miller, J.D. Jr., 2007. The Sonju Lake layered intrusion, northeast Minnesota: Internal structure and emplacement history from magnetic fabrics. Precambrian Research 157, pg. 269-288.

Miller, J.D., Jr. Green, J.C, Severson, M.J., Chandler, V.W., Hauck, S.A., Peterson, D.M., and Wahl, T.E., 2002, Geology and mineral potential of the Duluth Complex and related rocks of northeastern Minnesota: Minnesota Geological Survey Report of investigations 58, 207 p.

Miller Jr., J.D., Vervoort, J.D., 1996. The latent magmatic stage of the Midcontinent rift: a period of magmatic underplating and melting of the lower crust. Institute on Lake Superior Geology, 42nd Annual Meeting Proceedings Program and Abstracts 42, 33–35.

Miller, J.D., and Severson, M.J., 2002. Geology of the Duluth Complex, in Geology and mineral potential of the Duluth Complex and related rocks of northeastern Minnesota: Minnesota Geological Survey Report of Investigations 59, pp. 106-153.

Moskowitz, B.M., 1981. Methods for estimating Curie temperatures of titanomaghemites from experimentalJ_s-T data. Earth and Planetary Science Letters, Vol. 53, pg. 84-88.

Naslund, H.R., McBirney, A.R., 1996. Mechanisms of formation of igneous layering. In: Cawthorn, R.G. (Ed.), Layered Intrusions. Developments in Petrology 15, pg. 1–43.

Nicolas, A., 1992. Kinematics in magmatic rocks with special reference to gabbros. J. Petrol. 33, pg. 891–915.

O'Driscoll, B., Troll, V.R., Reavy, R.J., Turner, P., 2006. The Great Eucrite intrusion of Ardnamurchan, Scotland: reevaluating the ring-dike concept. Geology 34, pg. 189–192.

Paces, J.B., and Miller, J.D., 1993. Precise U-Pb Ages of the Duluth Complex and Related Mafic Intrusions, Northeastern Minnesota: Geochronological Insights to Physical, Petrogenetic, Paleomagnetic, and Tectonomagmatic Processes Associated With the 1.1 Ga Midcontinent Rift System. Journal of Geophysical Research, v. 98, pp. 13,997-14,013.

Peterson, D.M., 2001, Development of a conceptual model of Cu-Ni-PGE mineralization in a portion of the South Kawishiwi Intrusion, Duluth Complex, Minnesota: Laurentian University – Society of EconomicGeologists, Second Annual PGE Workshop, Sudbury,

Ontario

Peterson, D.M. and Albers, P.B., 2007, Geology of the Nickel Lake Macrodike and its association with Cu-Ni-PGE mineralization in the northern South Kawishiwi Intrusion, Duluth Complex, northeastern Minnesota: Institute on Lake Superior Geology, 53rd Annual Meeting, Trip #4, Field Trip Guidebook, Lutsen, Minnesota, Volume 53.

Peterson, D.M. 2008, Bedrock Geologic Map of the Duluth Complex in the Northern South Kawishiwi Intrusion and Surrounding Area, Lake and St. Louis Counties, Minnesota: Natural Resources Research Institute, Economic Geology Map Series NRRI/MAP-2008-01

Rochette, P., Aubourg, C., Perrin, M., 1999. Is this magnetic fabric normal? A review and case studies in volcanic formations. Tectonophysics 307, pg. 219–234.

Schwer, K., and Tauxe L., 2003, Characterization of soft-sediment deformation: Detection of cryptoslumps using magnetic methods, Geology, 31, 203–206.

Stephenson, A., 1994. Distribution anisotropy: two simple models for magnetic lineation and foliation. Phys. Earth Planet. Int. 82, pg. 49–53.

Swanson-Hysell, N.L., Maloof, A.C., Evans, D.A.D. and Weiss, B.P, 2009. No asymmetry in geomagnetic reversals recorded by 1.1-billion-year-old Keweenawan basalts. Nature Geoscience, p. 713-717.

Tarling, D.H. and F. Hrouda 1993. The Magnetic Anisotropy of Rocks. 1st ed., Chapman and Hall, London, New York, p. 217.

Tauxe, L., 1998. Paleomagnetic Principles and Practice. Modern approaches in Geophysics, vol. 17. Kluwer Academic Publishers, Dordrecht. 299 pp.

Tauxe, L. and K.P. Kodama, 2009, Paleosecular variation models for ancient times: Clues from Keweenawan lava flows, Phys. Earth Planet. Int., 177, 31-45.

Weiblen, P.W., 1965, A funnel-shaped gabbro-troctolite intrusion in the Duluth Complex, Lake County, Minnesota. Ph.D. thesis: University of Minnesota, p. 161.

Weiblen, P.W., Morey, G.B, 1980, A summary of the stratigraphy, petrology and the structure of the Duluth Complex: American Journal of Science, Vol. 280A, Part I, p. 88-133.

Zijderveld, J. D. A., 1967. A.C. demagnetization of rocks: Analysis of results, Methods in paleomagnetism, edited by D. W.Collinson, K. M. Creer, and S. K. Runcorn, pp. 254–286, Elsevier, New York.